

Arabidopsis HIPP proteins regulate endoplasmic reticulum-associated degradation of CKX proteins and cytokinin responses

Tianqi Guo^{1,2}, Henriette Weber¹, Michael C.E. Niemann¹, Lisa Theisl³, Georgeta Leonte¹, Ondřej Novák⁴ and Tomáš Werner^{3,*}

¹Institute of Biology/Applied Genetics, Dahlem Centre of Plant Sciences (DCPS), Freie Universität Berlin, Albrecht-Thaer-Weg 6, 14195 Berlin, Germany

²Guangdong Provincial Key Laboratory of Conservation and Precision Utilization of Characteristic Agricultural Resources in Mountainous Areas, School of Life Science of Jiaying University, 514015 Mei Zhou, China

³Institute of Biology, University of Graz, Schubertstraße 51, 8010 Graz, Austria

⁴Laboratory of Growth Regulators, Centre of the Region Haná for Biotechnological and Agricultural Research, Palacký University and Institute of Experimental Botany ASCR, 78371 Olomouc, Czech Republic

*Correspondence: Tomáš Werner (tomas.werner@uni-graz.at)

<https://doi.org/10.1016/j.molp.2021.07.015>

ABSTRACT

Eukaryotic organisms are equipped with quality-control mechanisms that survey protein folding in the endoplasmic reticulum (ER) and remove non-native proteins by ER-associated degradation (ERAD). Recent research has shown that cytokinin-degrading CKX proteins are subjected to ERAD during plant development. The mechanisms of plant ERAD, including the export of substrate proteins from the ER, are not fully understood, and the molecular components involved in the ERAD of CKX are unknown. Here, we show that heavy metal-associated isoprenylated plant proteins (HIPPs) interact specifically with CKX proteins synthesized in the ER and processed by ERAD. CKX–HIPP protein complexes were detected at the ER as well as in the cytosol, suggesting that the complexes involve retrotranslocated CKX protein species. Altered CKX levels in *HIPP*-overexpressing and higher-order *hipp* mutant plants suggest that the studied HIPPs control the ERAD of CKX. Deregulation of CKX proteins caused corresponding changes in the cytokinin signaling activity and triggered typical morphological cytokinin responses. Notably, transcriptional repression of *HIPP* genes by cytokinin indicates a feedback regulatory mechanism of cytokinin homeostasis and signaling responses. Moreover, loss of function of *HIPP* genes constitutively activates the unfolded protein response and compromises the ER stress tolerance. Collectively, these results suggest that HIPPs represent novel functional components of plant ERAD.

Guo T., Weber H., Niemann M.C.E., Theisl L., Leonte G., Novák O., and Werner T. (2021). *Arabidopsis* HIPP proteins regulate endoplasmic reticulum-associated degradation of CKX proteins and cytokinin responses. *Mol. Plant*. **14**, 1918–1934.

INTRODUCTION

The endoplasmic reticulum (ER) is the entry gate to the secretory pathway and serves as a dynamic protein-folding organelle where the ER-resident molecular chaperones and folding catalysts promote newly synthesized proteins to attain their native conformations (Strasser, 2018). Misfolding not only leads to protein dysfunction but also induces cellular toxicity. Therefore, the ER evolved a highly efficient ER quality control (ERQC) system to monitor an efficient and accurate folding process, recognizing non-native protein conformations for additional rounds of chaperone-assisted folding and targeting terminally misfolded proteins and unassembled proteins for ER-associated degradation (ERAD) (Berner et al., 2018). ERAD is a

conserved, multistep process involving the recognition of terminally misfolded proteins from folding intermediates, retrotranslocation from the ER to cytosol, polyubiquitination, and degradation by the ubiquitin-proteasome system (Strasser, 2018; Wu and Rapoport, 2018). Once the ERAD client proteins are recognized, they are brought to the membrane-anchored ERAD complexes for retrotranslocation and ubiquitination. In yeast, there are at least two such ERAD complexes differing in their core component, which is a membrane-embedded protein with a RING finger-type ubiquitin ligase (E3) activity

Published by the Molecular Plant Shanghai Editorial Office in association with Cell Press, an imprint of Elsevier Inc., on behalf of CSPB and CEMPS, CAS.

(Strasser, 2018). Because the catalytic domains of these E3 ligases are exposed to the cytosolic surface of the ER membrane, ERAD clients need to undergo retrotranslocation for ubiquitination and degradation by the cytosolic proteasome system. Despite considerable progress toward understanding the processes controlling biogenesis and degradation of ER proteins, the molecular mechanisms underlying the retrotranslocation and post-retrotranslocation steps of ERAD are not well defined (Hampton and Sommer, 2012).

The plant hormone cytokinin controls diverse developmental processes including cell proliferation and differentiation in meristems and forming organs, onset of senescence, and responses to biotic and abiotic signals (Werner and Schmölling, 2009; Zürcher and Müller, 2016). In the shoot, cytokinin plays a major role in maintaining proliferation of stem cells in the shoot apical meristem and has a positive effect on leaf initiation and development (Werner et al., 2003; Nishimura et al., 2004; Leibfried et al., 2005; Bartrina et al., 2011). Cytokinin controls the leaf size by sustaining the duration of the cell proliferation phase and by delaying the onset of cell differentiation in leaf primordia (Holst et al., 2011). Cytokinin is also involved in the maintenance of prolonged morphogenetic activity and formation of marginal serration and lobes (Rupp et al., 1999; Shani et al., 2010; Efroni et al., 2013). In contrast to its promoting role in shoot organs, cytokinin negatively controls root elongation and branching (Werner et al., 2003; Laplaze et al., 2007). Root elongation is determined by the activity of the root apical meristem where mitotic cell division is precisely balanced with differentiation of daughter cells. Cytokinin controls the rate of cell differentiation in the transition zone, a border between dividing and expanding cells (Werner et al., 2003; Dello Iorio et al., 2007).

Cytokinin signaling involves a His–Asp phosphorelay system, which is similar to the bacterial two-component signaling (TCS) systems for sensing environmental stimuli (Hwang and Sheen, 2001). The core cytokinin signaling cascade involves components that are encoded by multigene families, including *Arabidopsis* histidine kinase (AHK) receptors, histidine-containing phosphotransfer proteins, type-B response regulators (ARRs) regulating the transcriptional output from the phosphorelay, and type-A ARRs functioning as negative-feedback regulators of cytokinin signaling (Kieber and Schaller, 2018). The type-A ARRs are cytokinin primary response genes that can be used to monitor transcriptional activity in response to cytokinin (D'Agostino et al., 2000; Hwang and Sheen, 2001). The cytokinin signal is perceived by three AHK cytokinin receptors, which predominantly localize to the ER and, to a certain degree, to the plasma membrane (Caesar et al., 2011; Wulfetange et al., 2011), suggesting that the cytokinin signaling is initiated in the ER and apoplast, respectively. The functional relevance of the differential localization of AHK receptors as well as homeostatic control of cytokinin concentrations in the respective subcellular compartments is currently unclear (Zürcher et al., 2016; Romanov et al., 2018).

The maintenance of cytokinin homeostasis in individual tissues, cells, and organelles is dependent on biosynthesis, metabolic conjugation, degradation, and inter- and intracellular transport of the hormone. Cytokinin degradation is catalyzed by seven

FAD-containing cytokinin oxidase/dehydrogenase (CKX) enzymes in *Arabidopsis* (Schmölling et al., 2003). Individual CKX proteins are differentially localized and thereby control different subcellular cytokinin pools. While CKX7 is the single isoform acting in the cytosol (Köllmer et al., 2014), CKX1 to CKX6 are imported into the ER and further differentially targeted within the secretory system. The latter CKX proteins are apparently either retained in the ER or secreted into the apoplast (Werner et al., 2003; Niemann et al., 2018). As these CKX proteins likely colocalize with AHK receptors, it is apparent that their activity will control the pool of cytokinin, which is directly perceived by the receptors and triggers signaling responses. It has been recently shown that the levels of CKX proteins synthesized in the ER are controlled by ERQC, and the proteins undergo regulated degradation by the proteasome-dependent ERAD pathway (Niemann et al., 2015, 2018).

In this work, we report the identification of heavy metal-associated isoprenylated plant proteins (HIPPs) that connect the ERAD pathway with regulation of cytokinin responses. HIPPs are characterized by the presence of one or more heavy metal-associated (HMA) domains and C-terminal prenylation/farnesylation site. They are unique to vascular plants, and approximately 45 HIPPs are encoded in *Arabidopsis* (Barth et al., 2009; Tehseen et al., 2010; Supplemental Figure 1). A small number of HMA-containing proteins conserved in all eukaryotes function as metallochaperones delivering metal ions to specific metalloproteins and subcellular compartments (Robinson and Winge, 2010). In contrast, the biological function of the diversified HIPP family is largely unknown. The proteins have been suggested to act in heavy metal homeostasis and in adaptation to biotic and abiotic stresses (Suzuki et al., 2002; Barth et al., 2009; Gao et al., 2009; Tehseen et al., 2010; de Abreu-Neto et al., 2013; Zschiesche et al., 2015; Cowan et al., 2018).

Protein prenylation refers to post-translational lipid modification in which either a 15-carbon farnesyl or 20-carbon geranylgeranyl isoprenoid is linked via a thioether bond to specific cysteine residues of proteins containing a C-terminal prenylation site. In the case of farnesylation, this site is represented by a CaaX motif (where “C” is Cys, “a” is an aliphatic amino acid, and “X” is Met, Ala, Gln, Ser, or Cys) (Crowell and Huizinga, 2009). The prenylation reaction occurs in the cytosol and the modification enhances the interaction of the modified protein with the ER, where two additional processing steps—proteolytic removal of the “aaX” residues and carboxymethylation of the C-terminal Cys—take place (Resh, 2013). Attachment of hydrophobic lipid moieties to target proteins usually facilitate their interaction with membranes or other proteins (Hemsley, 2015). In plants, protein prenylation has been implicated in hormone signaling, cell division, and plant development (Crowell and Huizinga, 2009).

Here, we define the molecular function of several HIPPs in modulating ERAD activity and demonstrate that they likely affect retrotranslocation of CKX proteins targeted to ER and apoplast. Several lines of evidence demonstrated that the identified HIPPs determine the abundance of the active CKX protein species in the ER and thereby regulate cytokinin responses and plant development. This work provides important knowledge toward fully deciphering the function of the evolutionary young HIPP family in land plants.

RESULTS

CKX proteins interact with distinct members of the HIPP family

It has been previously shown that the cellular levels of CKX proteins are regulated by ERQC/ERAD, which significantly impacts on the cytokinin responses (Niemann et al., 2015). To explore further molecular mechanisms underlying this regulation, we searched for CKX-interacting proteins by conducting a yeast two-hybrid (Y2H) screen using CKX1 as bait. Coding sequences corresponding to six different HIPPs were recovered with high frequency (~65% of all isolated interactions; Supplemental Table 1). Interestingly, the isolated HIPPs fall into two phylogenetically distinct clades of the HIPP family: HIPP5, HIPP6, and HIPP7 belong to cluster I and HIPP32, HIPP33, and HIPP34 form a separate cluster III (Tehseen et al., 2010; Supplemental Figure 1). Full-length cDNAs corresponding to HIPP5, HIPP6, HIPP7, and HIPP34 were cloned and the interactions with CKX1 confirmed in one-on-one Y2H assays (Figure 1A).

To confirm that CKX1 interacts with HIPPs *in planta*, we transiently coexpressed myc-CKX1 with GFP-HIPP7 in *Nicotiana benthamiana* and used total protein extracts for coimmunoprecipitation (co-IP) assays. As shown in Figure 1B, myc-CKX1 was clearly detected in the GFP-HIPP7 immunocomplex, but it did not coimmunoprecipitate with GFP alone, supporting the notion of a direct CKX1–HIPP interaction. Similarly, myc-HIPP6 and myc-HIPP7 were coimmunoprecipitated when GFP-CKX1 was used as bait (Supplemental Figure 2A).

The Y2H screen suggested that only a specific subset of HIPPs forms complexes with CKX1. To further test this idea, we cloned additional members of the HIPP family and tested them for their interaction with CKX1. Figure 1A shows that HIPP1 and HIPP9, additional members of cluster I, interacted with CKX1. In contrast, randomly chosen HIPPs outside the clusters I and III, HIPP19 and HIPP35, showed no interaction with CKX1 in yeast (Figure 1A).

Next, we analyzed whether other CKX proteins are interacting partners of identified HIPPs. All tested HIPPs interacted strongly with CKX5 in yeast; the strongest interaction was conferred by HIPP6 (Supplemental Figure 2B). An apparently weaker interaction was observed between CKX2 and HIPP5, HIPP6, and HIPP7, and an even weaker interaction was detected between CKX4 and HIPP6 and HIPP7. Interestingly, CKX3 and CKX7 showed no interaction with tested HIPPs in Y2H assays. Together, the Y2H assays support the notion of promiscuous interactions between the ER/apoplast-localized CKX isoforms and HIPPs from specific subgroups of the HIPP family.

Isoprenylation of HIPP7 is essential for the interaction with CKX1

To understand the mechanism of CKX–HIPP interaction, we studied protein domains required for this interaction, taking the CKX1–HIPP7 complex as a case example. To test whether prenylation of HIPPs is relevant for CKX–HIPP complex formation, we mutated the prenyl-accepting Cys residue within the isoprenylation motif of HIPP7 (HIPP7^{C352G}; Figure 1C) and analyzed interaction of this mutant with CKX1. As shown in Supplemental Figure 2C, the mutation completely abolished the interaction in

yeast. Similarly, no interaction was detected using co-IP (Figure 1D), indicating that the prenylation of HIPP7 is required for the interaction with CKX1.

Several HIPPs, including HIPP7, were previously shown to bind various heavy metals via their HMA domain (Dykema et al., 1999; Suzuki et al., 2002). We mutated both HMA domains in HIPP7 by exchanging metal-binding Cys residues to glycines (HIPP7^{h^{ma}}; Figure 1C) and tested the resulting mutant variant for interaction with CKX1. Y2H and co-IP assays clearly showed that the interaction was not affected (Figure 1D and Supplemental Figure 2C), suggesting that metal binding is dispensable for CKX–HIPP interactions.

Next, we examined which CKX protein region mediates the interaction with HIPP by performing C-terminal deletion analysis of CKX1 (Figure 1E). Whereas truncation of CKX1 by 145 amino acids (CKX1⁴³⁰) did not strongly influence the interaction with HIPP7 (data not shown), deletion of 21 additional residues (CKX1⁴⁰⁹) strongly suppressed the yeast growth (Figure 1F). Similarly, the interaction of CKX1⁴⁰⁹ with other tested HIPPs was completely abolished or strongly reduced (Figure 1F), suggesting that the region between amino acid residues 409 and 430 is important for conferring the binding to HIPP. We examined this region for a sequence motif conserved among CKX proteins interacting with HIPP. The Asn-Ile-Leu-Thr (NILT) residues positioned in the short sequence stretch predicted to be exposed on the CKX1 protein surface were selected (Figure 1E and Supplemental Figure 2D). These residues were mutagenized in CKX1 to Asp-Leu-Val-Lys residues (CKX1^{421DLVK}), thus mimicking the sequence of CKX7 at this position. Y2H tests showed that the CKX1^{421DLVK} mutant can no longer or only weakly interact with HIPPs (Figure 1G), confirming the relevance of the 409–430 sequence region of CKX1 for the HIPP binding and suggesting that the mutated residues may be part of the interaction interface.

We next analyzed potential protein–protein interactions among the isolated HIPPs. HIPP7 showed homodimerization in yeast and in co-IP experiments, but did not interact with HIPP6 (Supplemental Figure 2F and 2G). Interestingly, the HIPP7 homodimerization was lost when the HIPP7^{C352G} and HIPP7^{h^{ma}} mutant variants were used, suggesting that both the protein isoprenylation and metal binding is essential for the HIPP7 homocomplex formation.

Subcellular localization of clade-I HIPPs

To gain insight into cellular mechanisms underlying the activity of HIPPs, we investigated their subcellular localization. HIPP7 and HIPP1 were fused to GFP at their N termini to avoid interference with the potential C-terminal prenylation, and the fusion proteins were expressed under the control of the 35S promoter in *N. benthamiana* leaf epidermis and in stably transformed *Arabidopsis*. Confocal microscopy revealed that GFP-HIPP7 was localized mainly in the cytoplasm of *N. benthamiana* cells, as indicated by a diffuse staining of the cytoplasmic strands and nucleoplasm (Figure 2A). However, in comparison with free mCherry cytoplasmic/nuclear marker, GFP-HIPP7 also accumulated at the nuclear envelope (Figure 2A, arrowhead) and less frequently within distinct puncta at the cell periphery (Supplemental Figure 3A); a pattern characteristic of plasmodesmal localization

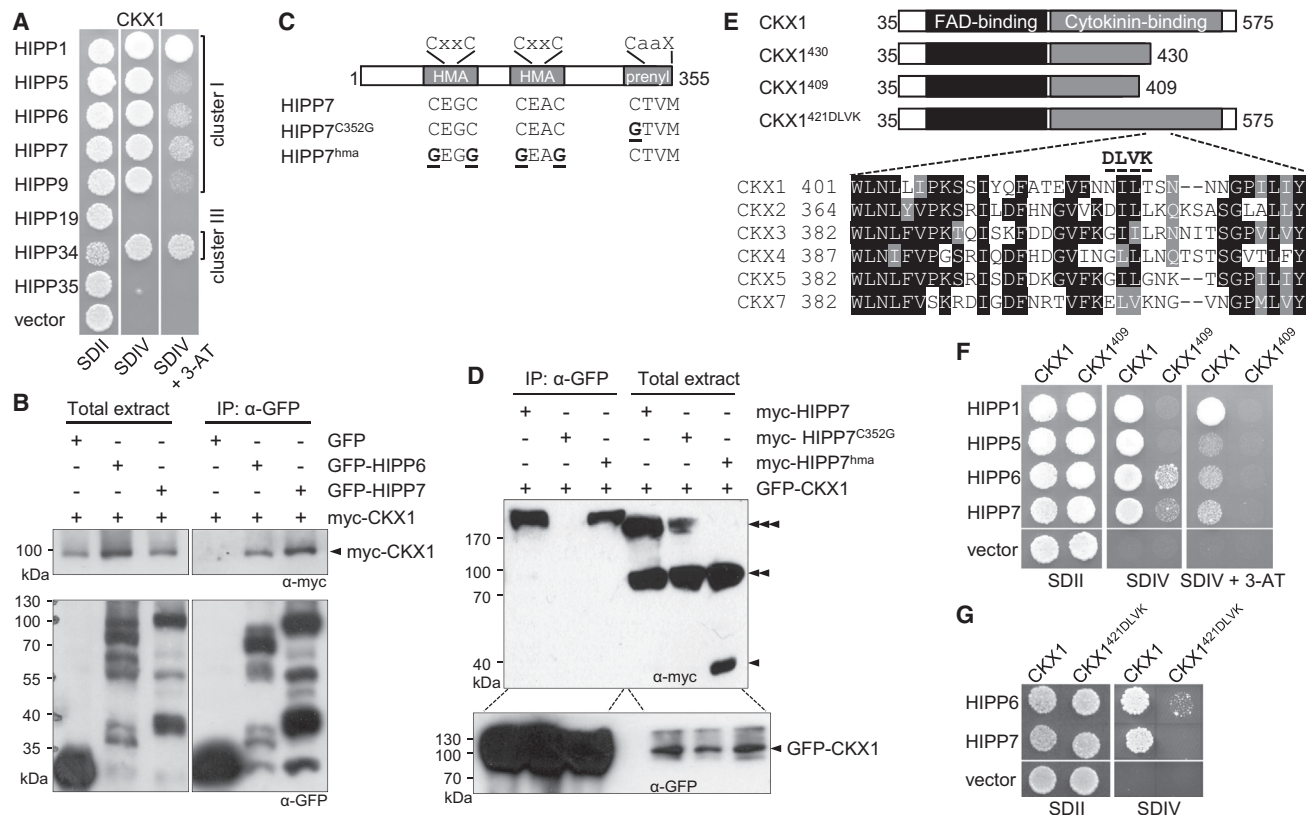


Figure 1. CKX1 and HIPPs interact in vitro and in vivo

(A) Interaction between CKX1 and HIPPs detected by yeast two-hybrid (Y2H) assays. Growth of yeast strains harboring CKX1 as bait and the indicated HIPPs as prey on control medium (SDII), interaction medium (SDIV), and SDIV supplemented with 3-amino-1,2,4-triazole (3-AT). Empty vector pACT2-GW was used as control.

(B) *In vivo* interaction of CKX1 with HIPPs. myc-CKX1 was transiently coexpressed with GFP-HIPP6, GFP-HIPP7, or GFP in *N. benthamiana*. Protein extracts were used for immunoprecipitations with anti-GFP antibody followed by immunoblotting with anti-myc and anti-GFP antibodies. The left panel shows the input (20 μg of crude extracts used for co-IP assay); the right panel shows the pellet fractions from co-IP.

(C) Scheme of HIPP7 protein structure with conserved motifs. Introduced mutations are indicated in bold/underlined.

(D) Co-IP assays reveal the loss of CKX1–HIPP7 interaction upon mutating isoprenylation site in HIPP7 (HIPP7^{C352G}), whereas mutation of HMA domains (HIPP7^{hma}) does not affect the interaction. Similar experimental setup as in **(B)** was used. Single, double, and triple arrowheads indicate the apparent monomeric, dimeric, and higher-order oligomeric forms of myc-HIPP7.

(E) Schematic representation of the CKX1 protein and its mutant variants used in the interaction assays. A segment of the sequence alignment of CKX proteins tested for the interaction with HIPPs covering the region with the introduced mutations (bold/underlined). The full-length CKX protein sequences were aligned using ClustalW.

(F) Interaction between the C-terminally truncated CKX1⁴⁰⁹ and HIPPs is strongly reduced in Y2H assay.

(G) The mutation of CKX1 at positions 421–424 (CKX1^{421DLVK}) abolishes the interaction with HIPP6 and HIPP7 in yeast.

(Oparka et al., 1997; Yuan et al., 2016). In the cortical region, GFP-HIPP7 showed cytosolic localization adjacent to the ER network labeled with the coexpressed ER marker protein RFP-p24 (Lerich et al., 2011) (Figure 2B). Colocalization of GFP-HIPP7 with RFP-p24 was observed with low occurrence (Figure 2C). In contrast, GFP-HIPP7^{C352G} mutant form lacking the prenylation site was localized mainly to the cytosol, and the signal was apparent neither at the ER nor plasmodesmata. Similar subcellular localization of GFP-HIPP7 was detected in stably transformed *Arabidopsis*; however, in comparison with the *N. benthamiana* system, the protein labeled plasmodesmata more strongly (Supplemental Figure 3C). Interestingly, the frequency of plasmodesmal localization was lower and the fluorescence signal associated with plasmodesmata was significantly weaker in *Arabidopsis* plants expressing GFP-HIPP7^{C352G} (Supplemental Figure 3D). In contrast, GFP-HIPP7^{C352G} showed increased occurrence in the

cytosol, suggesting that prenylation is largely required for the localization of HIPP7 to plasmodesmata. However, the weak plasmodesmal localization of GFP-HIPP7^{C352G} in *Arabidopsis* suggests that other targeting determinants might be involved.

The GFP-HIPP1 fusion protein expressed in *N. benthamiana* was localized mainly in the cytoplasm and nucleus (Figure 2D). In the nucleus, the fluorescence labeled nucleoplasm and small bright foci, which were usually localized to nucleolus (Figure 2E). With lower frequency, the GFP-HIPP1 fluorescence was also associated with plasmodesmata (Figure 2D, inset). Comparable subcellular localization of GFP-HIPP1 was observed also in the transgenic *Arabidopsis* plants (Supplemental Figure 3E); however, the frequency and intensity of the GFP-HIPP1 signal at the plasmodesmata was significantly stronger than in *N. benthamiana*.

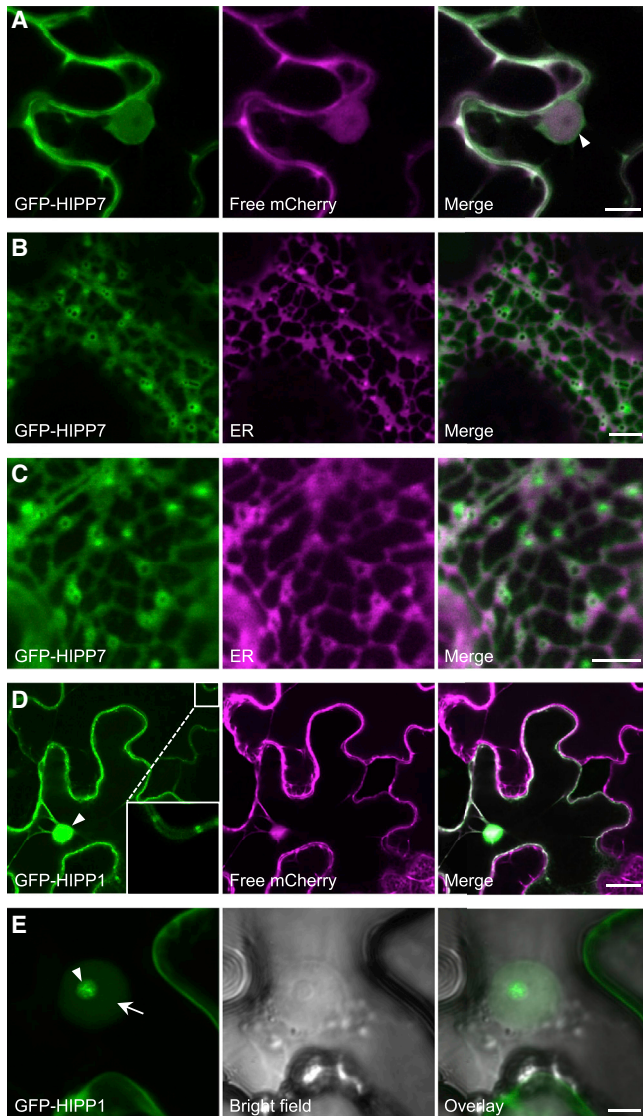


Figure 2. Analysis of the subcellular localization of GFP-HIPP7 and GFP-HIPP1 fusion proteins in *N. benthamiana*

(A–C) Confocal microscopy analysis of *N. benthamiana* leaf epidermal cells transiently expressing *35S::GFP-HIPP7*. In the central plane of the cell, the protein is detected in the cytosol (pCambia-mCherry, magenta), in the nucleoplasm, and at the nuclear membrane (arrowhead) (A). In the cell cortex, GFP-HIPP7 localizes mainly adjacent to the ER (RFP-p24, magenta) (B); less frequently, they colocalize (C).

(D and E) Representative confocal microscopy images of *N. benthamiana* leaf epidermal cells coexpressing *35S::GFP-HIPP1* with the cytosolic marker (magenta). GFP-HIPP1 localizes in the nucleus (arrowhead) and in the cytoplasm. Occasionally, GFP-HIPP1 fluorescence was associated with plasmodesmata (magnified in the inset) (D). In the nucleus, the GFP-HIPP1 fluorescence labels the nucleoplasm (arrow) and small bright foci within the nucleolus (arrowhead) (E).

Scale bars represent 10 μm (A), 5 μm (B, C, and E), and 25 μm (D).

Microscopic analysis suggested that the examined HIPPs might exist in different forms, as cytosolic and as being associated with other cellular structures such as the ER and plasmodesmata. To substantiate this notion and gain further insight into the basic cellular properties of the HIPPs, we studied the solubility and possible membrane association of the GFP-HIPP7 protein stably

expressed in *Arabidopsis* under the control of the *UBIQUITIN10* (*UBQ10*) promoter (Geldner et al., 2009). Cellular protein fractionation followed by protein gel blot analysis revealed that GFP-HIPP7 was predominantly associated with microsomal membranes and almost absent in the supernatant fraction of soluble proteins (Supplemental Figure 3F). Interestingly, the apparent molecular mass of GFP-HIPP7 was higher than expected for the GFP-HIPP7 monomer, suggesting that HIPP7 is part of a larger molecular complex, which was not fully resolved under SDS-PAGE conditions. Importantly, in contrast to GFP-HIPP7, the membrane association of the mutant form lacking the prenylation site (GFP-HIPP7^{C352G}) was strongly reduced, indicating that the prenylation is one important factor for attaching HIPP7 to membranes.

HIPPs interact with the CKX1 protein exported from the ER

Previous studies have demonstrated that CKX proteins, identified in this work as interacting with HIPPs, are localized to various compartments of the secretory pathway including mainly the ER and apoplast (Werner et al., 2003; Niemann et al., 2018). In view of the described CKX–HIPP interactions, it is therefore intriguing that HIPP1 and HIPP7 apparently localize on the cytosolic side of the ER and plasma membrane, raising the question about cellular mechanisms underlying these protein–protein interactions.

To address this, we tested CKX1–HIPP7 interaction using bimolecular fluorescence complementation (BiFC) (Gookin and Assmann, 2014). CKX1 and HIPP7 were fused at their N termini to the N- and C-proximal halves of the Venus fluorescent protein (NVen and CVen, respectively). To monitor non-specific assembly of NVen and CVen, we used the parent vector expressing NVen-CKX1 together with unfused CVen as control. As illustrated in Figure 3A, no or very weak BiFC was detected in the cells expressing the control vector. In contrast, all cells expressing NVen-CKX1 and CVen-HIPP7 showed strong Venus fluorescence (Figure 3B), indicating BiFC between the fusion proteins and suggesting that CKX1 and HIPP7 interact also *in planta*. GFP-HIPP7^{C352G} did not interact with CKX1 in the BiFC assay (Figure 3C and Supplemental Figure S4A), confirming the hypothesis that post-translational protein modification is required for the complex formation.

Most interestingly, in contrast to GFP-HIPP7 predominantly localized to cytosol (Figure 2), the fluorescence of the NVen-CKX1/CVen-HIPP7 complex clearly localized to the cortical and perinuclear ER and small punctate structures (Figure 3F and Supplemental Figure 4B). This pattern closely resembled the subcellular localization of CKX1-GFP (Niemann et al., 2018). The BiFC experiments thus indicate that the CKX1–HIPP7 complex formation involves specifically the ER-associated HIPP7 protein fraction (Figure 2C), or that the protein–protein interaction increases the affinity of HIPP7 to the ER membrane. Most importantly, we have previously shown that CKX1 exhibits a transmembrane topology with the C terminus residing in the ER lumen (Niemann et al., 2018). Given that the CKX1 domain mediating the interaction with HIPPs is localized in the luminal part of the protein (Figure 1 and Supplemental Figure 4C), BiFC between CKX1 and HIPP7 implicates that the CKX1 protein in the

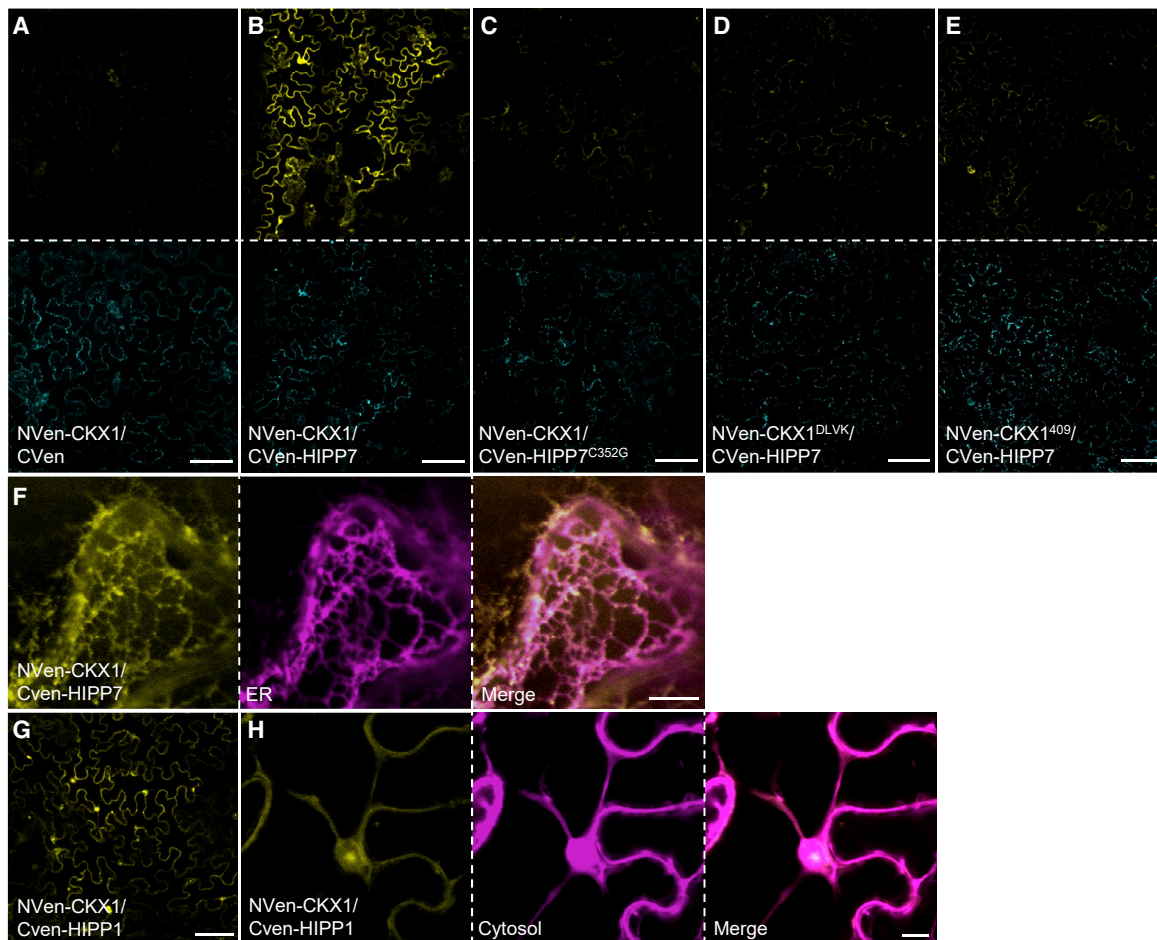


Figure 3. CKX1 interacts with HIPPs in planta

(A–E) Confocal microscopy analysis of bimolecular fluorescence complementation assay (BiFC) in *N. benthamiana* epidermal leaf cells expressing the NVen-CKX1/CVen parent vector control **(A)** and the indicated CKX1/HIPP7 protein pairs **(B–E)**. Upper images show the Venus-derived fluorescence (yellow); lower images show the expression controls as indicated by mTq2 fluorescence.

(F) NVen-CKX1/CVen-HIPP7 BiFC fluorescence signal localizes to the cortical ER and small punctate structures. Yellow, Venus BiFC; magenta, RFP-p24.

(G and H) Reconstitution of the Venus-derived fluorescence demonstrates NVen-CKX1 interaction with CVen-HIPP1 **(G)**. NVen-CKX1/CVen-HIPP1 BiFC (yellow) signal is distributed mainly in the nucleus and weakly in the cytoplasm, as indicated by the colocalization with pCambia-mCherry (magenta) **(H)**. Scale bars represent 100 μm **(A–E and G)** and 10 μm **(F and H)**.

detected complex represents a form which was relocated to the cytosolic side of the membrane. This is consistent with the recent finding that CKX1 is targeted to the ERAD pathway (Niemann et al., 2015), which requires retrotranslocation of target proteins from the ER prior to delivery to the cytosolic/nuclear proteasome (Hampton and Sommer, 2012). To test whether CKX1–HIPP7 interaction involves the retrotranslocated CKX1 protein, we performed BiFC assays using CKX1^{421DLVK} and CKX1⁴⁰⁹ that were unable to interact with HIPPs in yeast. As shown in Figure 3D and 3E and Supplemental Figure S4A, no interaction was detected between HIPP7 and these two CKX1 mutant variants, corroborating the idea that HIPP7 interacts with the luminal domain of CKX1 during or upon retrotranslocation from the ER. The results therefore implicate a function of HIPP7 during retrotranslocation or post-retrotranslocation processing of CKX1.

As shown in Figure 3G, a clear BiFC signal was detected also for the NVen-CKX1/CVen-HIPP1 pair. The fluorescence signal was

mainly localized in the nucleus and cytoplasm (Figure 3H), suggesting that the complex also involves the retrotranslocated cytosolic CKX1 fraction. However, unlike NVen-CKX1/CVen-HIPP7, the NVen-CKX1/CVen-HIPP1 complex was not detected at the ER, suggesting that it was detached from the ER membrane upon CKX1 retrotranslocation.

Overexpression of clade-I HIPP genes causes pleiotropic phenotypes and alters cytokinin responses in a prenylation-dependent manner

To explore the physiological function of the isolated HIPPs, we first performed gain-of-function experiments by expressing selected GFP-HIPPs under the 35S promoter in *Arabidopsis*. Individual transgenic lines expressing 35S:GFP-HIPP6 and 35S:GFP-HIPP7 (called 35S:HIPP6 and 35S:HIPP7 hereafter) developed very similar pleiotropic phenotypes that have not been observed previously (Suzuki et al., 2002). Transgenic lines expressing either construct developed smaller rosette leaves

with strongly altered morphology, which correlated with the expression levels of the respective transgene (Figure 4 and Supplemental Figure 5). Similar, yet more severe, changes in leaf development resulted from overexpression of *GFP-HIPP1* under the *UBQ10* promoter (Supplemental Figure 5), suggesting that clade-I *HIPP* genes might generally display similar activity in controlling leaf development. The transgenic leaves were characterized by shorter petioles and smaller lamina with serrated and crinkly leaf margins (Figure 4B). These morphological changes were reminiscent of those observed in cytokinin-overproducing plants or mutants with an increased expression of class-1 *KNOX* homeobox genes (Chuck et al., 1996; Rupp et al., 1999). As leaf size and shape are determined by patterns of cell division and cell expansion, we analyzed the cell size of epidermal cells in the fully developed *35S:HIPP7* rosette leaves. Microscopic analysis revealed a strongly increased number of the *35S:HIPP7* epidermal cells, which were reduced in size by ~60% in comparison with wild type (Figure 4C). Moreover, whereas differentiated adaxial epidermal pavement cells of wild-type plants had a characteristic puzzle-shape morphology, the *35S:HIPP7* cells developed much less convoluted shape with fewer lobes and indentations (Figure 4D), indicating a delayed differentiation. This notion was corroborated by the frequent occurrence of apparently recent cell-division events in the expanded *35S:HIPP7* leaves (Figure 4D, arrowheads).

Next, we examined whether the extended proliferation and delayed leaf maturation reflect altered cytokinin responses in the *HIPP*-overexpressing plants. To this end, we increased the endogenous cytokinin content in the analyzed plants by treatment with the CKX inhibitor INCYDE (Zatloukal et al., 2008) and analyzed the leaf growth responses. Figure 4E and 4F show that the wild type responded to the low INCYDE concentration by increasing the leaf area, which is typical for plants treated with low cytokinin concentrations (Efroni et al., 2013) or displaying enhanced cytokinin activity (Bartrina et al., 2017). In contrast, the leaf areas of *35S:HIPP6* and *35S:HIPP7* were reduced in response to already low INCYDE concentration, and the reduction was significantly stronger after treatment with higher concentrations than in wild type. Moreover, the crinkly leaf phenotype was strongly enhanced after the inhibitor treatment (Figure 4E). Together, these results suggest that the *35S:HIPP6* and *35S:HIPP7* plants are hypersensitive to cytokinin.

To test the effect of *HIPP* expression on cytokinin sensitivity in more detail and to avoid the strong leaf morphological changes associated with *35S:HIPP* expression, we generated transgenic lines expressing *GFP-HIPP7* under the control of the *UBQ10* promoter (*UBQ10:HIPP7*). Selected lines displayed no detectable changes in leaf morphology under the control conditions (Supplemental Figure 6A). Nevertheless, the *UBQ10:HIPP7* leaves responded more sensitively than the wild type toward INCYDE (Figure 4G), corroborating the notion of increased cytokinin sensitivity through *HIPP* expression. Most importantly, the hypersensitive responses were completely abolished in plants expressing the *GFP-HIPP7* mutant form lacking the prenyl-accepting site (*UBQ10:HIPP7^{C352G}*; Figure 4G and Supplemental Figure 6). These data suggest that the CKX–*HIPP* complex formation enhanced by *HIPP7* expression was likely causal for the enhanced cytokinin sensitivity.

Notably, an increased sensitivity toward cytokinin was observed also in the generated *UBQ10:HIPP1* lines (Supplemental Figure 6D), suggesting that the ability to modulate cytokinin responses may be common to clade-I *HIPP*s.

The altered development of *HIPP*-overexpressing plants is causally linked to enhanced cytokinin activity

To further explore the cytokinin effect on the development of *HIPP*-expressing plants, we crossed *35S:HIPP7* plants with *repressor of cytokinin deficiency4 (rock4)*, which is a dominant gain-of-function mutation of the cytokinin biosynthesis *isopentenyltransferase 3 (IPT3)* gene with increased endogenous cytokinin content (I. Bartrina, T. Werner, and T. Schmölling, unpublished data). This mutant was isolated based on its ability to suppress the cytokinin deficiency (Niemann et al., 2015). Figure 5A illustrates that the elevated cytokinin biosynthesis severely enhanced the *35S:HIPP7* leaf developmental defects, corroborating the enhanced cytokinin sensitivity of the transgenic line.

Next, we analyzed whether the phenotypic changes in *HIPP*-overexpressing plants were reflected by the content of endogenous cytokinins. The analysis revealed that the contents of most cytokinin metabolites were relatively weakly changed in the transgenic plants (Supplemental Tables 2 and 3). The strongest changes were detected for isopentenyladenine (iP) and *trans*-zeatin (tZ) nucleotides, which were reduced to about 70% of the wild-type levels. In contrast, concentrations of cytokinin O-glucosides were significantly increased. Interestingly, in contrast to iP- and tZ-type cytokinins, all *cis*-zeatin metabolites were increased in all transgenic lines. Together, the complex changes of the cytokinin profiles indicate that a number of homeostatic reactions were activated in response to the expression of different *HIPP* genes.

Because of the subtle changes of cytokinin concentrations, we directly analyzed the cytokinin status of the *HIPP1*- and *HIPP7*-overexpressing plants by introgressing the cytokinin output sensor *TCSn:GFP* (Zürcher et al., 2013). Since the *TCSn:GFP* reporter displays a relatively low fluorescence signal in rosette leaves, we analyzed its expression levels by qRT-PCR. Figure 5B shows that *TCSn:GFP* expression was significantly increased in the transgenic lines. These results correlate with the increased sensitivity toward cytokinin and suggest that clade-I *HIPP*s increase cytokinin activities.

To further corroborate these results, we analyzed the expression of type-A *ARR* genes encoding the downstream component of the cytokinin signaling pathway (To et al., 2004). qRT-PCR analysis revealed an upregulation of *ARR5* and *ARR7* in *HIPP*-overexpressing plants (Supplemental Figure 7A). Interestingly, the steady-state transcript levels of most analyzed *ARR*s were unaltered or decreased in comparison with wild type, suggesting their differential regulation in response to *HIPP* expression. Notably, among the downregulated type-A *ARR*s were genes previously shown to be specifically expressed in the expanding leaves to inhibit cytokinin responses and cell proliferation (Efroni et al., 2013). For example, the *ARR15* and *ARR16* were strongly downregulated in *HIPP*-overexpressing leaves, and the reduction was progressively stronger during the later stages of leaf

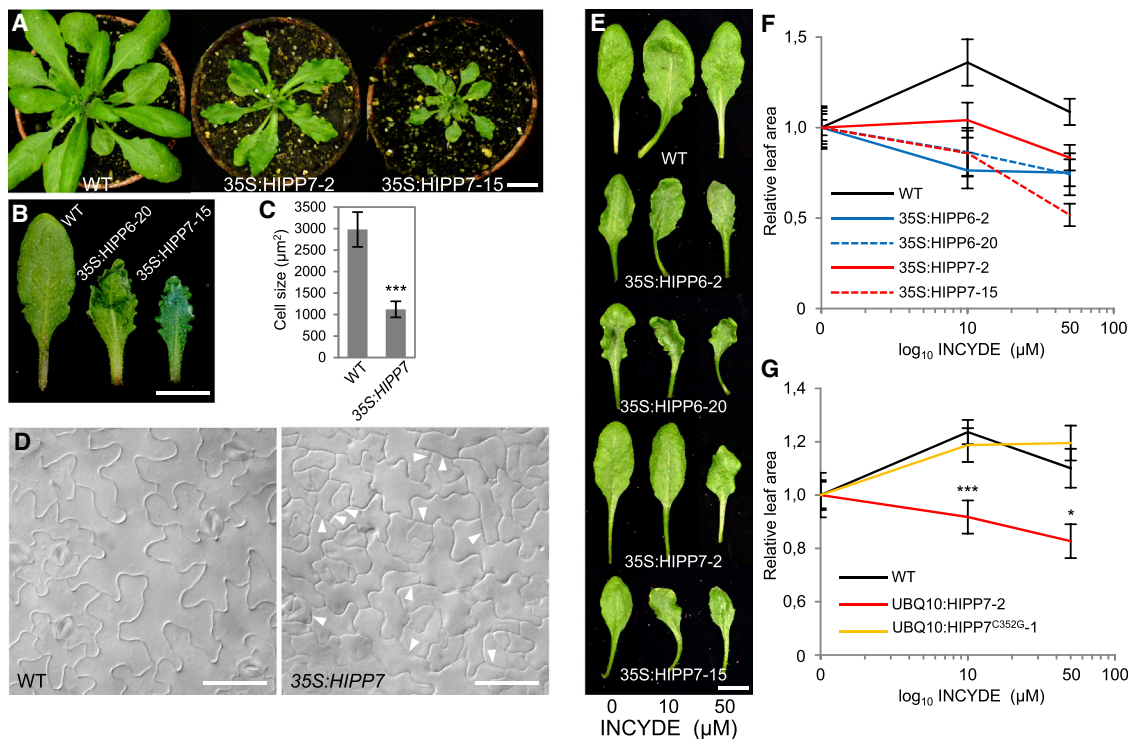


Figure 4. Overexpression of clade-I HIPP genes alters leaf development and enhances cytokinin responses

(A) Four-week-old wild-type (WT) and *35S::GFP-HIPP7*-expressing plants. Two independent lines are shown.

(B) Morphology of the sixth rosette leaf of plants shown in (A) and Supplemental Figure 5A.

(C) Average size of abaxial epidermal cells of the fifth and sixth rosette leaves of the WT and *35S::HIPP7-15* line at 28 days after germination (DAG). Data are mean \pm SD ($n \geq 15$). *** $P < 0.005$, calculated by Student's t -test.

(D) Abaxial epidermis of the sixth leaf of plants analyzed in (C). Cells at 25% distance from tip to base are shown. Examples of apparently recently formed cell walls are indicated by arrowheads.

(E) Leaf 7 from WT and two independent homozygous lines expressing *35S::HIPP6* and *35S::HIPP7* treated repeatedly with INCYDE (10 and 50 μ M) for 4 weeks.

(F) Relative growth of rosette leaf 7 of plants shown in (E). Data are mean \pm SE ($n = 8-9$). All mutant lines differed significantly from WT for both INCYDE treatments (Student's t -test, $P < 0.05$, false discovery rate [FDR]-corrected).

(G) Relative growth of rosette leaf 7 of WT and *UBQ10::HIPP7* and *UBQ10::HIPP7^{C352G}* plants treated as in (E). Data are mean \pm SE ($n = 8$). * $P < 0.05$, *** $P < 0.005$, calculated by FDR-corrected Student's t -test.

Scale bars represent 1 cm (A, B, and E) and 50 μ m (D).

maturation (Supplemental Figure 7B), which correlates with the appearance of the severe leaf developmental defects in the transgenic plants. Hence, the diminished expression of these *ARRs* correlates with the higher *TCSn::GFP* activity and enhanced cytokinin responsiveness in *HIPP*-overexpressing plants.

To test whether the enhanced cytokinin activity is causally involved in the establishment of the *HIPP*-overexpression phenotype, we crossed *35S::HIPP6* to *35S::ARR15*, which displays reduced cytokinin sensitivity (Ren et al., 2009). As shown in Figure 5C and Supplemental Figure 7, the *35S::HIPP6* phenotype was significantly suppressed, indicating that the altered leaf development in *HIPP*-overexpressing plants is largely caused by enhanced cytokinin activity.

Next, we analyzed the potential activity of the selected *HIPP* genes during root development. We observed that the *UBQ10::HIPP1* lines, which displayed the most severe changes in shoot morphology, also developed a strongly retarded root system. The primary root elongation and lateral root formation was severely impaired in correlation with the transgene expression

(Supplemental Figure 8A and 8B). As cytokinin regulates cell differentiation in the root apical meristem, we analyzed the root meristem size in different *UBQ10::HIPP1* lines by scoring the number of the meristematic cortex cells. The cell number was strongly reduced in *UBQ10::HIPP1* meristems (Supplemental Figure 8C), indicating premature cell differentiation and suggesting that the altered root meristem activity was due to enhanced cytokinin responses. In agreement with this, the *TCSn::GFP* activity was significantly enhanced in *UBQ10::HIPP1* meristems; the GFP signal was stronger in the procambial cells and expanded upward into the root vasculature in comparison with control (Figure 5E and Supplemental Figure 8D).

Since we showed that prenylation of HIPP7 was necessary for the establishment of the overexpression phenotypes in leaves, we further tested whether this post-translational protein modification is also important for HIPP activity in roots. Figure 5F and 5G show that the transgenic line expressing *UBQ10::HIPP7* displayed significantly reduced (~10%) elongation of the primary root and formation of the lateral roots (~20%). Importantly, the

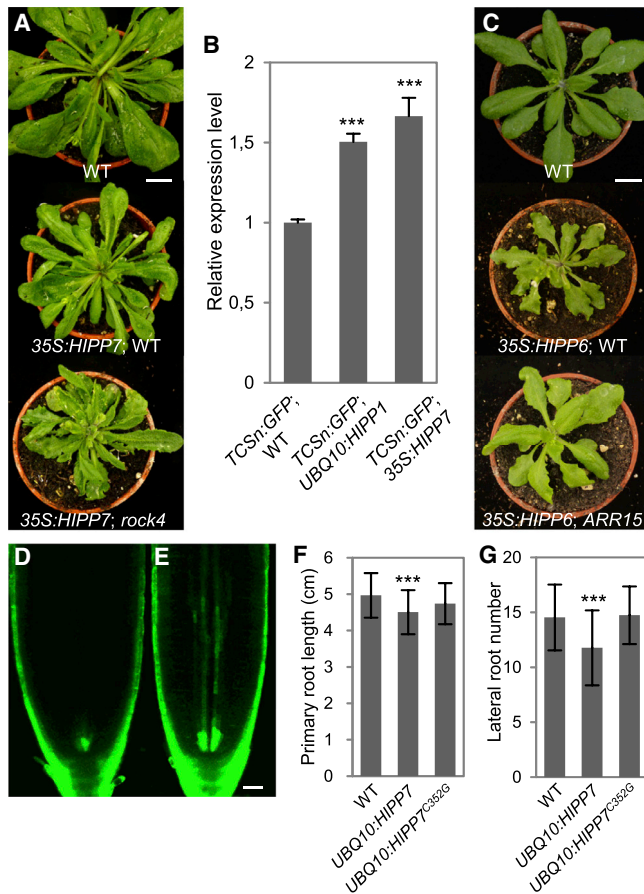


Figure 5. Abnormal development of HIPP-overexpressing lines is largely caused by an enhanced cytokinin activity

(A) A dominant gain-of-function mutation of the cytokinin biosynthesis *IPT3* gene (*rock4*; repressor of cytokinin deficiency4) enhances the *35S:HIPP7* leaf developmental defects. Note the reduced leaf size and extensive serration in the hybrid plants. F1 hybrid plants at 28 DAG are shown.

(B) qRT-PCR analysis of *GFP* transcript levels in rosettes of 15-DAG F1 plants from the crosses between *TCSn:GFP* with wild-type (WT), *UBQ10:HIPP1-19*, and *35S:HIPP7-15* plants. Data are mean \pm SE ($n = 3$). *** $P < 0.005$, calculated by FDR-corrected Student's *t*-test.

(C) Suppression of the altered leaf morphology of *35S:HIPP6* plants by the expression of *35S:ARR15*. F1 hybrid plants at 23 DAG are shown.

(D and E) Confocal microscopy of root meristems of F1 plants of *TCSn:GFP* crossed with WT (D) and *UBQ10:HIPP1-19* (E). Images were captured using identical confocal settings. Note that the background GFP fluorescence corresponding to the GFP-HIPP1 protein expressed in *UBQ10:HIPP1* lines was very low (Supplemental Figure 8D) and thus did not interfere with analysis of the *TCSn:GFP* activity.

(F) Length of the primary root of the WT and plants expressing *UBQ10:GFP-HIPP7* and *UBQ10:GFP-HIPP7^{C352G}*. Root elongation between days 3 and 10 after germination. Data are mean \pm SD ($n = 30$). *** $P < 0.005$, calculated by FDR-corrected Student's *t*-test.

(G) Number of emerged lateral roots in plants shown in (F) at 10 DAG. Data are mean \pm SD ($n = 30$). *** $P < 0.005$, calculated by FDR-corrected Student's *t*-test.

Scale bars represent 1 cm (A and C) and 25 μ m (D and E).

expression of *UBQ10:HIPP7^{C352G}* did not produce a significant change in root development, suggesting that the changes in cytokinin activity in roots were dependent on HIPP7 prenylation.

HIPPs alter the ERAD of CKX and provide feedback control of cytokinin activity

The described phenotypic and molecular analysis provided several indications that cytokinin activity was increased due to HIPP overexpression. Moreover, as the BiFC assays provided indications that the HIPPs may function in the ERAD of CKX proteins, we asked whether the enhanced cytokinin activity in HIPP overexpressors is linked to a perturbed function of CKX proteins. To approach this question, we crossed the *UBQ10:HIPP1*, *35S:HIPP6*, and *35S:HIPP7* with a transgenic line expressing CKX1-myc, a well-studied ERAD substrate (Niemann et al., 2015), under the *Arabidopsis thaliana* MERISTEM LAYER 1 (*ATML1*) promoter. Analysis of the *ATML1:CKX1-myc*, *UBQ10:HIPP1* F1 progenies revealed that the CKX1-myc levels were strongly reduced in comparison with the control cross (Figure 6A and Supplemental Figure 9), suggesting that the CKX1-HIPP1 interaction triggers degradation of CKX1. These results correlate with the enhanced cytokinin activity in the HIPP1-overexpressing plants.

In contrast, CKX1-myc levels were significantly increased upon the expression of *35S:HIPP6* and *35S:HIPP7* (Figure 6A and Supplemental Figure 9A), suggesting that CKX1-myc was stabilized in the complex with the respective HIPPs and/or the HIPPs impeded some steps of the ERAD pathway. Notwithstanding the mechanism, the increased cytokinin activity in HIPP6 and HIPP7 overexpressors implicate that the accumulated CKX1-myc protein was physiologically non-functional and that less cytokinin degradation occurred in the ER lumen.

To test this assumption, we crossed *35S:myc-CKX1* to the *ubs7* mutant, which has been identified to prevent degradation of several ERAD substrates (Liu et al., 2015). Figure 6B shows that *ubs7* completely suppressed the cytokinin-deficient growth phenotype, indicating that EBS7 controls negatively cytokinin activity. Intriguingly, the myc-CKX1 levels were strongly increased (Figure 6C and Supplemental Figure 9C), suggesting an accumulation of biologically inactive myc-CKX1 paralleled by a loss of its activity in the ER. These results correlate with the data obtained from HIPP6- and HIPP7-overexpressing plants, and together support the idea that disturbance of ERAD may result in accumulation of a substrate protein and yet cause the loss of its function in the ER at the same time.

To gain more insights into the role of HIPPs in regulating cytokinin responses, we isolated insertion mutant alleles of individual HIPP genes and generated a set of higher-order mutants by genetic crosses (Supplemental Figure 10). The *pATML1:CKX1-myc* construct was introduced into the *hipp5 hipp6 hipp7* triple mutant (referred to as *hipp5,6,7* hereafter), and the CKX1-myc levels were assessed. The analysis revealed that *hipp5,6,7* significantly reduced the CKX1-myc abundance and accordingly also suppressed the cytokinin-deficient shoot growth phenotype (Figure 6D and 6E). These data, therefore, strongly support the role of HIPPs in maintaining CKX levels. To understand the relevance of this regulation under physiological conditions, we examined root growth and cytokinin activity in different *hipp* multiple mutants. Supplemental Figure 10 shows that the primary root growth and lateral root development were reduced in two examined triple and *hipp5,6,7,8* quadruple mutants.

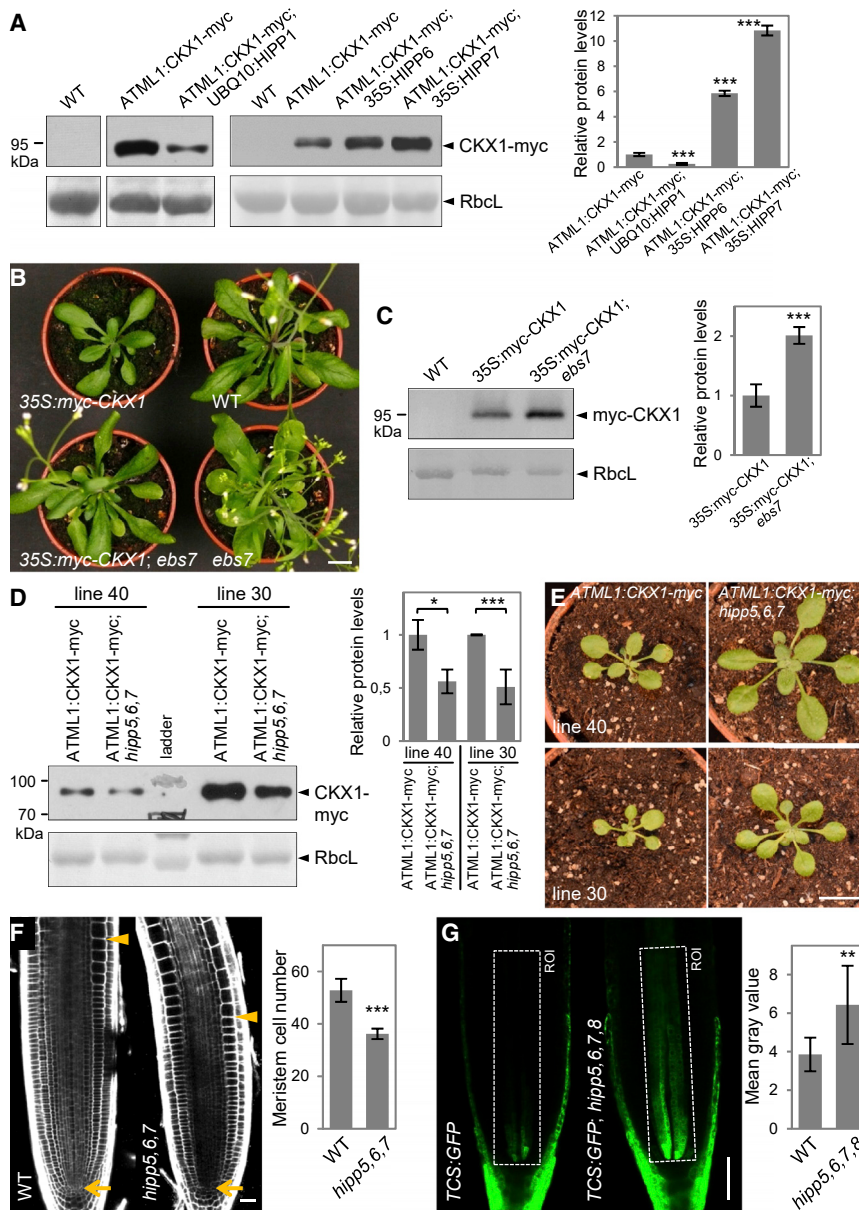


Figure 6. Regulation of CKX1 protein levels in HIPP-overexpressing plants and ERAD mutants

(A) Comparison of the CKX1-myc protein abundances in F1 plants resulting from crosses between the *ATML1:CKX1-myc Arabidopsis* line and plants expressing *UBQ10:HIPP1*, *35S:HIPP6* and *35S:HIPP7*. Hemizygous F1 plants from the cross between *ATML1:CKX1-myc* and wild type (WT) were used as a control. Protein extracts (30 μ g) from shoots were analyzed by immunoblotting with anti-myc antibody. Coomassie blue staining of Rubisco large subunit (RbcL) was used as loading control. Relative densitometric analysis of the CKX1-myc signal is shown. Data are mean \pm SD ($n = 4$). $***P < 0.005$ (one-way ANOVA with post hoc Tukey–Kramer test). The transcript levels of the *CKX1* transgene were comparable in the hybrid and control plants (Supplemental Figure 9).

(B) The *ebs7* mutation suppresses the cytokinin-deficient shoot phenotype of *35S:myc-CKX1* plants (26 DAG). Scale bar represents 1 cm.

(C) myc-CKX1 protein levels are increased in *35S:myc-CKX1 ebs7* hybrid plants. Protein analysis was performed as in (A). Relative densitometric analysis of the myc-CKX1 signal is shown. Data are mean \pm SD ($n = 4$). $***P < 0.005$ (one-way ANOVA with post hoc Tukey–Kramer test).

(D) CKX1-myc levels in WT and *hipp5,6,7* plants. *ATML1:CKX1-myc* was transformed into the homozygous *hipp5,6,7* mutant and independent transformation events were selected. Two selected T1 plants (lines 30 and 40) were crossed to WT and *hipp5,6,7*, and the progenies heterozygous and homozygous, respectively for *hipp5,6,7* were selected. The *ATML1:CKX1-myc* allele was hemizygous in both genotypes compared. Immunoblot analysis was performed as in (A). Relative densitometric analysis of the CKX1-myc signal is shown. Data are mean \pm SD ($n = 3$). $*P < 0.05$, $***P < 0.005$ (one-way ANOVA with post hoc Tukey–Kramer test).

(E) *hipp5,6,7* suppresses the cytokinin-deficient shoot phenotype caused by *ATML1:CKX1-myc*. Same plants as used for the analysis in (D) are depicted at 15 DAG. Scale bar represents 1 cm.

(F) Root meristem size in WT and *hipp5,6,7* plants at 7 DAG. Arrows indicate the QC, and arrowheads indicate the cortex cell at the transition zone. Scale bar represents 25 μ m. Cells in a cortex cell file between the QC and transition zone were counted. Data are mean \pm SD ($n = 10$). $***P < 0.005$, calculated by Student’s *t*-test.

(G) Confocal microscopy analysis of *TCSn:GFP* in root meristems of WT and *hipp5,6,7,8* mutant. White boxes indicate region of interest (ROI) used for the quantification of the *TCSn:GFP* signal. Scale bar represents 50 μ m. Data are mean \pm SD ($n = 20$). $**P < 0.01$, calculated by Student’s *t*-test.

The decreased root elongation correlated with reduced size of the root apical meristem (Figure 6F), indicating that the examined HIPP proteins play a positive role in root growth control. The root growth in individual *hipp* single and double mutants was comparable with that in wild type (data not shown), indicating a high degree of functional redundancy among clade-I HIPP genes. Analysis of the *TCSn:GFP* reporter introgressed into the *hipp5,6,7,8* mutant revealed a significantly enhanced cytokinin signaling activity in comparison with wild type, which was particularly expanded in the stele of the proximal meristem toward the transition zone (Figure 6G). Correlating with this observation, the transcript levels of several type-A *ARR* genes were strongly elevated in *hipp* triple and

quadruple mutants (Supplemental Figure 10G). These results further support the conclusion that clade-I HIPP proteins are physiologically important regulators of cytokinin response.

We next asked whether the HIPP function is controlled by cytokinin. To this end, we assessed the transcriptional regulation of clade-I HIPP genes by cytokinin using qRT–PCR. After 30 min of cytokinin treatment, the *HIPP5*, *HIPP6*, and *HIPP7* transcript levels were downregulated to about 40% relative to control plants (Supplemental Figure 11). Interestingly, the expression was restored to normal levels after 2 h of treatment. This fast and transient regulation suggests that these HIPP genes are

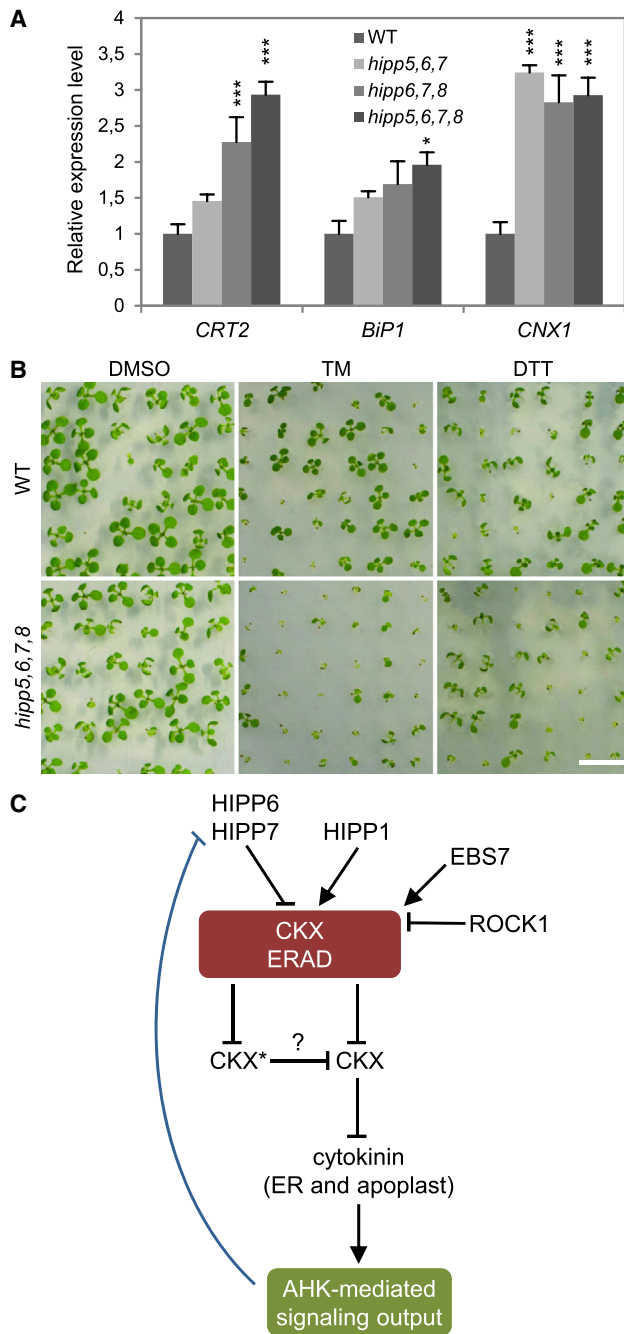


Figure 7. HIPPs are involved in ERAD and ER stress responses

(A) qRT-PCR analysis of UPR gene expression in rosettes of plants at 15 DAG. Data are mean \pm SE ($n = 4$). * $P < 0.05$, *** $P < 0.005$, calculated by FDR-corrected Student's t -test.

(B) Seedlings grown on half-strength MS medium supplemented with DMSO (control), tunicamycin (TM), or dithiothreitol (DTT) for 8 days. One representative image of at least three independent experiments including both WT and *hipp5,6,7,8* mutant with ~ 40 seedlings each is shown. Scale bar represents 1 cm.

(C) A proposed model illustrating how HIPPs function in regulating cytokinin responses. Cytokinin is perceived by AHK receptors localized to the ER and apoplast. The steady-state concentrations of cytokinin in these compartments are regulated by ER-localized and secretory CKX proteins. These CKX proteins are monitored by ERQC to attain their biochemically competent conformation (CKX). Our data predict that the misfolded pro-

teins (CKX*) as well as partially misfolded, but biochemically competent, species are degraded by ERAD. Experiments with *ews7* and *HIPP6* and *HIPP7* gain-of-function plants suggest that accumulation of CKX* affects the CKX activity and cytokinin degradation. The protein-protein interactions with HIPPs modulate the CKX ERAD, and the reduction of HIPP activity results in less cytokinin degradation in the ER and apoplast, which triggers cytokinin-related transcriptional responses. This includes a fast transcriptional repression of *HIPPs* (blue line), triggering a positive regulatory loop, which further attenuates cytokinin degradation and reinforces the cytokinin signal.

Loss of function of HIPPs activates the UPR and reduces ER stress tolerance

Recent studies have shown that mutations of ERQC/ERAD components constitutively trigger the unfolded protein response (UPR) (Hüttner et al., 2014; Liu et al., 2015). To further assess the physiological functions of HIPPs and to test whether the *hipp* mutations activate the UPR, we measured the transcript levels of ER-resident proteins that are typically activated to alleviate ER stress (Howell, 2013). The analysis showed that the expression of *Binding protein 1 (BiP1)*, *Calnexin 1 (CNX1)*, and *Calreticulin 2 (CRT2)* was significantly increased in *hipp* triple and quadruple mutant plants (Figure 7A), indicating that the loss of HIPP causes ER stress and constitutive activation of the UPR pathway. The increase in UPR prompted us to investigate the stress tolerance of the mutants. We grew seedlings on medium supplemented with tunicamycin (TM) and dithiothreitol (DTT), widely used ER stress-inducing agents. Compared with the wild type, the *hipp* quadruple mutant displayed markedly increased sensitivity indicated by the higher percentages of dying and dead seedlings on TM/DTT-containing media (Figure 7B and Supplemental Figure 12). These data are in good agreement with the proposed role of HIPPs in the modulation of the plant ERAD processes.

DISCUSSION

HIPPs interact with the ER- and apoplast-localized CKXs in a prenylation-dependent manner

The HIPPs identified in this study are characterized by their ability to form complexes with CKX proteins that are imported via their N-terminal targeting domains to the ER. After initial processing in the ER, these CKX proteins are either retained in the ER or exported to the apoplast (Werner et al., 2003; Niemann et al., 2018), where they control the subcellular pools of cytokinins that represent the direct input signal perceived by the AHK receptors (Romanov et al., 2018). The interactions were specific toward these ER/apoplastic CKXs, because the cytosolic CKX7 did not interact with any of the tested HIPPs. Interestingly, the subcellular localization of GFP-HIPP1 and GFP-HIPP7 contrasts in part with the localization of their CKX-interacting partners. The proteins were mainly detected in the

HIPP proteins function in ERAD

cytosol, nucleus, and, in part, at the ER membrane. As the HIPPs are likely post-translationally modified by prenylation, the detected subcellular localizations of GFP-HIPPs are in good agreement with the known biogenesis route of proteins undergoing this lipid modification. However, whereas GFP-HIPP1 is likely a soluble protein, as indicated by its localization to the cytosol/nucleoplasm, GFP-HIPP7 was partially localized to ER in *N. benthamiana*. In agreement with this, GFP-HIPP7 was predominantly associated with microsomal membranes in *Arabidopsis*. The comparatively weak ER localization of GFP-HIPP7 in *N. benthamiana* as detected by confocal microscopy was likely due to occurrence of untargeted GFP fragments resulting from the partial degradation of the GFP-HIPP7 that was detected by immunoblot analyses. It is, however, not excluded that only a fraction of GFP-HIPP7 was prenylated and attached to the ER membrane because of limiting prenylation capacity in *N. benthamiana* cells. Importantly, the membrane binding of GFP-HIPP7^{C352G} was reduced, indicating that the attachment to endomembranes is partially dependent on the prenylation. However, the non-prenylated GFP-HIPP7 protein still showed significant membrane binding, suggesting that other factors are involved. Prenylation generally provides a relatively weak membrane anchor and usually requires an additional signal to facilitate stable membrane attachment (Hemsley, 2015). In line with this, the S-acylation of NbHIPP26 has been shown to be important for its localization to the plasma membrane (Cowan et al., 2018). Interestingly, we observed that GFP-HIPP7 and GFP-HIPP1 proteins partially localized to plasmodesmata, although the significance of this currently remains unclear.

HIPPs regulate the CKX ERAD process

The subcellular localization of the formed BiFC complexes largely correlated with those of the individual GFP-HIPPs. The CKX1-HIPP7 BiFC complex localized at the cortical and perinuclear ER and small punctate structures, whereas the CKX1-HIPP1 complex was soluble as evidenced by its cytoplasmic/nuclear localization. These results, together with the fact that CKX1 is an ER-resident protein (Niemann et al., 2018), indicate that the HIPPs interact with CKX1 exported from the ER lumen to the cytosolic side of the ER membrane. This hypothesis is strongly supported by the work of Niemann et al. (2015) who have demonstrated that the ER/apoplastic CKXs are ERAD substrates. Because the catalytic domain of the core component of the ERAD complex is on the cytosolic surface of the ER membrane, it is required to retrotranslocate the ERAD substrates to the cytosol to undergo ubiquitination (Berner et al., 2018). An export of CKX1 from the ER prior the interaction with HIPPs was corroborated by the finding that the interaction domain is in the CKX1 C terminus, which is oriented to the ER lumen (Niemann et al., 2018).

The interaction with the retrotranslocated ERAD substrates indicates that the identified HIPPs likely represent plant-specific components of the ERAD system. This finding is in line with growing evidence that *Arabidopsis* ERAD involves not only proteins evolutionarily conserved in eukaryotes but also components specific to plants (Liu et al., 2015; Lin et al., 2019). The mechanism of how the isolated HIPPs connect to ERAD of CKXs is currently unclear. Overexpression of all tested HIPPs

increased cytokinin responses, suggesting that the HIPP likely modulated the ERAD of the interacting endogenous ER/apoplastic CKX proteins (Figure 7C). This is supported by the finding that CKX1-myc levels were reduced upon coexpression with *UBQ10:HIPP1*, suggesting that HIPP1 promotes the ERAD of its interacting proteins and that the increased cytokinin responses were due to reduced CKX activity in the ER. Intriguingly, cytokinin responses were also similarly enhanced in plants overexpressing HIPP6 and HIPP7, yet the CKX1-myc levels were increased. These data suggest that different HIPPs might regulate different steps of ERAD. Supported by the subcellular localization of different BiFC complexes, we hypothesize that HIPP6 and HIPP7 control more upstream processes such as the retrotranslocation at the membrane, whereas HIPP1 promotes downstream steps of ERAD such as escorting the substrate proteins to the proteasome. These differences might be dictated by the subcellular localization features of individual HIPPs. The cytosolic/nuclear HIPP1 contains a predicted nuclear localization signal (amino acids 100–122 based on gene model of At2g28090.2; cNLS Mapper; Kosugi et al., 2009). The nuclear localization signal might function as a driving force that promotes the CKX-HIPP complex accessing the proteasome. The outcome of the *HIPP6* and *HIPP7* activity in plants is not easy to interpret. The surprising increase in CKX1-myc levels by HIPP6 and HIPP7 proposes their negative function in the ERAD of CKX (Figure 7C). However, the paradoxical increase of cytokinin responses indicated that the accumulated CKX1-myc protein was biologically inactive. This idea is supported by analysis of the *ebs7* mutation (Liu et al., 2015) which, in similar manner, increased myc-CKX1 levels while enhancing cytokinin response, as manifested by the suppression of the cytokinin-deficient phenotype. EBS7 is a plant-specific ER membrane protein regulating stability of HMG-CoA reductase degradation1 (Hrd1) (Liu et al., 2015). Hrd1, the ER membrane-anchored ubiquitin E3 ligase, is the core structural component of the multiprotein complex that degrades different ERAD substrates in yeast. Hrd1 likely represents the protein-conducting channel for the retrotranslocation of ERAD clients (Baldrige and Rapoport, 2016), and a similar role is discussed for Hrd1 in plants (Strasser, 2018). The *ebs7* mutation in *Arabidopsis* destabilizes Hrd1 and causes accumulation of ERAD substrates (Liu et al., 2015), which is consistent with the myc-CKX1 accumulation observed in this work. The loss of biological activity of myc-CKX1 could be the result of the accumulation of the defective protein to the disfavor of the correctly folded and active CKX1 protein species in the ER. Alternatively, given the functionally relevant homodimerization of CKX1 (Niemann et al., 2018), the accumulation of the misfolded protein might cause a dominant-negative effect on the myc-CKX1 in *ebs7*. Similar effects on CKX1 levels and activity in *HIPP6* and *HIPP7* overexpression backgrounds are, therefore, consistent with the proposed function of these HIPPs in regulating more upstream steps of the CKX ERAD pathway. The model proposing a negative role of HIPP6 and HIPP7 in the ERAD of CKX proteins (Figure 7C) is in full agreement with reduction of CKX1-myc levels observed in the higher-order mutant comprising *hipp6* and *hipp7* alleles. Nevertheless, it remains to be studied how HIPPs execute their function. It will be, for example, important to understand whether HIPPs function exclusively through the interaction with the ERAD substrate proteins or whether they also interfere with the components of the ERAD machinery.

CKX–HIPP interaction modulates cytokinin signaling output to regulate plant growth and development

The cytokinin signal is perceived by AHK receptors, which localize to plasma membrane and to the ER (Caesar et al., 2011; Wulfetange et al., 2011). The current model predicts that the bulk of cytokinin signaling is initiated from the ER and the cellular response is determined by the steady-state concentration of the hormone in the ER lumen (Romanov et al., 2018). This work provides evidence that the CKX–HIPP protein–protein interactions represent a new homeostatic mechanism controlling the CKX activity in the ER and, thereby, cytokinin responses. As discussed above, different HIPPs likely modulate different steps of the CKX ERAD pathway, either directly influencing the CKX degradation or modulating the levels of the biologically active CKX proteins in the ER lumen. Both of these activities ultimately result in changes of cytokinin signaling through the ER-localized AHKs. In addition to the ER-resident CKX1, other CKX isoforms that are presumably secreted are apparently also controlled by ERAD (Niemann et al., 2015). Likewise, these CKXs undergo interaction with HIPPs, suggesting that ERAD of these CKX isoforms may determine their export rate from the ER and that the CKX–HIPP interaction module is relevant also for the apoplastic cytokinin pool.

Multiple lines of evidence supporting the HIPP function in controlling cytokinin responses are presented in this study. *TCSn:GFP* activity was significantly increased in *HIPP* overexpressors, and the plants were hypersensitive to exogenous cytokinin. Genetic analyses confirmed that the enhanced cytokinin status was causal for the overexpression phenotypes because the morphological changes were suppressed and enhanced by repressing the cytokinin signaling and enhancing the cytokinin biosynthesis, respectively. Moreover, in line with the reduced CKX levels, the investigated *hipp* multiple mutants displayed enhanced cytokinin responses, providing additional evidence for the functional relevance of the *HIPP* genes in regulating developmental processes governed by cytokinin.

Importantly, our work revealed fast and transient repression of the clade-I *HIPP* gene expression by cytokinin. The rapid downregulation indicates that these genes are likely cytokinin primary response genes. Based on the results from the loss-of-function experiments, which suggest that the true physiological role of the respective *HIPP* genes is to alleviate cytokinin responses, the transcriptional repression of these genes by cytokinin apparently constitutes a positive regulatory feedback loop in the cytokinin regulatory system (Figure 7C). The transient nature of the *HIPP* transcriptional regulation is typical for many immediate-early cytokinin responses (D'Agostino et al., 2000) and suggests a dynamic control of cytokinin by the HIPP-regulatory module. This feedback mechanism is predicted to transiently reinforce the cytokinin concentrations. Further investigations, however, are needed to understand in which physiological and developmental context this mechanism is particularly relevant. Interestingly, the CKX levels are regulated by another feedback mechanism involving transcriptional induction of the corresponding genes by cytokinin (Werner et al., 2006; Brenner et al., 2012), indicating that the cytokinin concentration in the ER/apoplast

undergoes a tight regulation underlay by an independent mechanism.

Given the changes of CKX levels in the *HIPP* overexpressors, it is interesting that the overall contents of endogenous cytokinin metabolites were changed relatively weakly. This suggested that different homeostatic mechanisms were activated in response to the enhanced cytokinin activity. Indeed, we detected that the expression of *IPT1*, *IPT3*, and *IPT5* genes was strongly reduced in all *HIPP*-overexpressing lines (Supplemental Figure 13), which is consistent with the transcriptional downregulation of these genes by cytokinin (Miyawaki et al., 2004). This result therefore indicates that the cytokinin biosynthesis was partially suppressed as a result of increased cytokinin signaling. In agreement with this, the levels of cytokinin nucleotides, which represent the primary products of cytokinin biosynthesis (Sakakibara, 2006), were reduced in *HIPP*-expressing lines. In the same line of evidence, the cytokinin *O*-glucosylation, which mitigates cytokinin activity (Bajguz and Piotrowska, 2009), was increased, suggesting that the enhanced conjugation may have compensated for the impaired cytokinin degradation. It is interesting that, in contrast to the enhanced cytokinin signaling, the overall concentrations of active cytokinins were not significantly altered in *HIPP* overexpressors. Comparably mild changes were detected in *rock1* plants displaying enhanced CKX ERAD (Niemann et al., 2015). These results may imply that the cytokinin pool in the ER is relatively small compared with the content of the whole cell and that the current analytical methods provide only limited information in this regard.

HIPPs function in mitigating ER stress

Although many changes caused by *HIPP* overexpression were causally linked to altered cytokinin activity, the pleiotropic phenotypic changes may suggest that the *HIPP* functions are, in part, exerted through cytokinin-independent pathways. Indeed, genetic analysis employing the *hipp* higher-order loss-of-function mutants revealed the functional involvement of *HIPPs* in processes necessary to mitigate ER stress. Misfolded proteins accumulate in the ER under adverse environmental conditions, causing potentially cell damage and compromising the plant survival (Howell, 2013). This triggers the UPR to limit the deleterious protein aggregation. Constitutive activation of the UPR pathway and greatly compromised tolerance of *hipp* mutants to ER stress show that the identified *HIPP* genes play a vital role in maintaining protein homeostasis in the ER. However, it needs to be studied whether and how specific environmental stress responses are controlled by the identified *HIPPs*. Given the numerous functions of cytokinin in diverse abiotic and biotic stress processes (Cortleven et al., 2019), it is appealing to speculate that *HIPPs* eventually couple the cytokinin action and ER stress response pathway during these processes. Lastly, it will be important to understand the functional diversification among *HIPPs* from different clades of the family. It is interesting that several *HIPP* genes have been reported to be involved in plant responses to biotic and abiotic stresses (Barth et al., 2009; Zschiesche et al., 2015; Cowan et al., 2018; Radakovic et al., 2018), although the underlying mechanisms have not been fully revealed.

METHODS

Plant materials and growth conditions

A. thaliana ecotype Columbia-0 was used as the wild type. The following lines were described previously: 35S:ARR15 (Ren et al., 2009), TCSn:GFP (Zürcher et al., 2013), *eps7-2* (Liu et al., 2015), *rock4* (I. Bartrina, T. Werner, and T. Schmölling, unpublished data), and *ATML1:CKX1-myc* (Werner et al., 2021). The T-DNA insertion mutants SALK_069207 (*hipp5-1*), SALK_111020C (*hipp6-1*), SALK_091924C (*hipp7-1*), and SM_3_25 599 (*hipp8-1*) were obtained from the Nottingham Arabidopsis Stock Centre. *Arabidopsis* plants were grown *in vitro* on half-strength Murashige and Skoog (MS) medium containing 10 g/l sucrose or in the greenhouse under long-day conditions (16 h light/8 h dark; 21°C/18°C). *N. benthamiana* plants were grown at 24°C under 14-h light/10-h dark conditions in the greenhouse.

Generation of gene constructs for expression in plants

To generate the binary destination vectors for driving the gene expression by the *UBQ10* promoter, we PCR-amplified and cloned the *UBQ10 promoter* into the Gateway destination vector pB7WGF2 (Karimi et al., 2002) via *HindIII/Spel* sites, replacing the cauliflower mosaic virus (CaMV) 35S promoter (the final vector is called pB7WGF2UBQ10).

For the *HIPP1*-overexpressing constructs, a cDNA sequence corresponding to the full-length cDNA clone AY924752 was amplified. The amplified fragment represents an alternative *HIPP1* gene model (At2g28090.2) starting within the second exon of the At2g28090.1 gene model. A cDNA corresponding to At2g28090.1 as annotated by TAIR10 was not recovered in multiple RT-PCR reactions. The *HIPP1* cDNA was cloned into pDONR221 (Invitrogen) and subsequently subcloned by Gateway LR recombination into the pB7WGF2UBQ10 vector for expression in *Arabidopsis* as well as into pK7WGF2 for subcellular localization studies. *HIPP6* and *HIPP7* cDNAs were first cloned into pDONR221 and subsequently subcloned by Gateway LR recombination into pK7WGF2 and pGWB18 (Earley et al., 2006) for expressing GFP- and myc-fusion proteins, respectively. The *HIPP7*^{C352G} and *HIPP7*^{hma} mutations were introduced by the QuikChange site-directed mutagenesis kit (Stratagene), confirmed by sequencing, and subcloned from pDONR221 into pB7WGF2UBQ10.

For the BiFC assays, *HIPP1* and *HIPP7* cDNAs and their mutant variants were amplified by PCR and cloned into the *KflI* site of MCS3 in pDOE-08-CKX1 (Niemann et al., 2018), resulting in different pDOE-08-CKX1-HIPP constructs, expressing CKX1 N-terminally tagged with the N-terminal fragment of monomeric Venus split at residue 210 (NVen-CKX1) and HIPP N-terminally tagged with the C-terminal Venus fragment (CVen-HIPP) (Gookin and Assmann, 2014). All primers used for cloning are listed in Supplemental Table 4. The binary vector constructs were transformed into *Arabidopsis* plants by an *Agrobacterium tumefaciens* (strain GV3101:pMP90) mediated floral dip method (Clough and Bent, 1998).

Y2H analysis

Corresponding cDNAs encoding CKX1, 2, 3, 4, and 7 were cloned into pDONR221 using primers listed in Supplemental Table 4 and subcloned into destination vectors pACT2 (prey) and pBTM116-D9 (bait) as described by Weber et al. (2005). CKX1 to CKX4 were cloned without N-terminal signal peptide/signal anchor sequences (Niemann et al., 2018) (<http://www.cbs.dtu.dk/services/SignalP>) to avoid targeting to the secretory pathway. pACT2-CKX5 clone coding for CKX5 fragment starting with the residue Cys17 at the N terminus was isolated from the prey-encoding pACT2 cDNA library (Dortay et al., 2008). Y2H assays were performed as described previously (Weber et al., 2005; Weber and Hellmann, 2009). SDII selection medium supplemented with Ura and His was used as transformation control, whereas SDIV minimal medium without Ura and His, or SDIV supplemented with 10 mM 3-AT, was used for interaction tests. Photographs were taken 5 days after plating.

Transient expression in *N. benthamiana* and confocal laser scanning microscopy

Gene constructs were transformed as described previously (Sparkes et al., 2006; Niemann et al., 2018) using *A. tumefaciens* strain GV3101:pMP90 and 6-week-old *N. benthamiana* plants. For coexpression, the *Agrobacterium* cultures were mixed in infiltration medium to a final OD₆₀₀ of 0.1 for each construct. 35S:p19 (Voinnet et al., 2003) was included in all infiltrations at OD₆₀₀ 0.1. RFP-p24 (Lerich et al., 2011) and pCambia-mCherry (Dalal et al., 2015) were used as markers. Confocal imaging analysis was performed using a Leica TCS SP5 laser scanning confocal microscope 1–3 days after infiltration as described by Niemann et al. (2018).

Protein analysis, co-IP assays, and membrane association analysis

For standard protein expression analysis, frozen plant material was homogenized and incubated in extraction buffer (50 mM Tris [pH 7.5], 150 mM NaCl, 0.3% Triton X-100, 1 mM phenylmethylsulfonyl fluoride). Crude extracts were centrifuged for 10 min at 6000 g (4°C). Supernatant was subjected to bicinchoninic acid assay or Bradford assay to measure protein concentration. Proteins (amount as indicated) were separated by 9%–10% SDS-PAGE and blotted on polyvinylidene fluoride membrane (Millipore). Membranes were blocked with 5% skim milk in PBS containing 0.1% Tween 20. A mouse monoclonal anti-myc antibody (clone 4A6; Millipore, dilution 1:1000) followed by a goat anti-mouse antibody coupled to horseradish peroxidase (HRP) (sc-2005; Santa Cruz Biotechnology, dilution 1:5000) was used to detect myc-CKX1 and CKX1-myc. The detection of GFP was performed with the anti-GFP antibody (JL-8; Clontech, dilution 1:2000) in conjunction with the secondary anti-mouse antibody. Bound antibodies were visualized with SuperSignal West Pico chemiluminescent substrate (Thermo Scientific). Respective GFP- and myc-fusion proteins were coexpressed transiently in *N. benthamiana* leaves and co-IP assays were performed as described previously (Niemann et al., 2018). The microsomal membranes were isolated from 10-day-old *Arabidopsis* seedlings by ultracentrifugation according to Niemann et al. (2018).

RNA extraction, cDNA synthesis, and qPCR

Whole RNA was extracted from tissues using a plant RNA extraction kit according to the manufacturer's manual (Machery & Nagel). RNA (2–3 µg) was transcribed into cDNA by Superscript III reverse transcriptase (Invitrogen) using 2.5 µM 25-mer oligo-dT primer and 4.5 µM 9-mer random primer. cDNA (75 ng) was used as template in a qPCR reaction consisting of 0.01 U/µl Immolase DNA-Polymerase (BioLine), the corresponding 1× buffer, 2 mM MgCl₂, 100 µM each deoxynucleotide triphosphate, 0.1× SYBR Green I (Fluka), 50 nM ROX (Sigma), and 300 nM each primer (Supplemental Table 4). qPCR analysis was performed using a 7500 Fast Real-Time PCR system (Applied Biosystems). The qPCR temperature program consisted of the following steps: 95°C for 15 min; 40 cycles of 95°C 15 s, 55°C 15 s, 72°C 15 s; followed by melting curve analysis. Two housekeeping genes (*PP2AA2* and *UBC10*) were used as a control to normalize the relative transcript abundances of each gene of interest according to Vandesompele et al. (2002).

Microscopy

Abaxial epidermis of the sixth leaf of 28-day-old plants grown on soil was analyzed by microscopy as described in Holst et al. (2011). For the root meristem size analysis, roots were stained with 10 µM propidium iodide, imaged with confocal microscopy, and the number of cortex cells scored as described previously (Dello Ioio et al., 2007).

Hormone and chemical treatments

For cytokinin treatment, 10 plants of each genotype were sprayed at 3-day intervals for 4 weeks with *N*⁶-benzyladenine (50 µM), CKX inhibitor IN-CYDE (10 and 50 µM) (Zatloukal et al., 2008; Niemann et al., 2015), or mock (0.05% dimethyl sulfoxide [DMSO]) after the first two leaves appeared. 0.01% Silwet L-77 was included in all treatments. The fully

expanded leaf 7 was photographed and the leaf area measured with ImageJ software (<http://imagej.nih.gov/ij/>). For the study of ER stress tolerance, seedlings were grown on half-strength MS medium supplemented with 60 $\mu\text{g/l}$ TM (Sigma), 1.5 mM DTT (Roche), or DMSO (control) for 8 days and the numbers of seedlings that were green (alive), yellowish (dying), or dead were counted and recorded.

Cytokinin measurements

The cytokinin contents in shoots of soil-grown plants at different developmental stages were determined by ultra-performance liquid chromatography–electrospray tandem mass spectrometry as described by Svačinová et al. (2012), including modifications described by Antoniadou et al. (2015).

Bioinformatics analysis

The protein secondary structure and solvent accessibility was predicted using the REPROFsec and PROFacc method, respectively, at the Predict-Protein server (<https://www.predictprotein.org>) (Rost et al., 2004).

ACCESSION NUMBERS

Sequence data from this article can be found in the GenBank/EMBL libraries under the following accession numbers and as specified in Supplemental Table 1 and Supplemental Figure 1: CKX1 (At2g41510), CKX2 (At2g19500), CKX3 (At5g56970), CKX4 (At4g29740), CKX5 (At1g75450), CKX7 (At5g21482), HIPP1 (At2g28090), HIPP5 (At2g36950), HIPP6 (At5g03380), HIPP7 (At5g63530), HIPP9 (At5g24580), HIPP19 (At3g21490), HIPP32 (At3g05220), HIPP33 (At5g19090), HIPP34 (At3g06130), and HIPP35 (At1g56210).

SUPPLEMENTAL INFORMATION

Supplemental Information is available at *Molecular Plant Online*.

FUNDING

This work was supported by grants from the Austrian Science Fund (P 30945), Deutsche Forschungsgemeinschaft (WE 4325/1-1 and WE 4325/2-2), and from the Ministry of Education, Youth and Sports of the Czech Republic (European Regional Development Fund-Project "Plants as a tool for sustainable global development" no. CZ.02.1.01/0.0/0.0/16_019/0000827).

AUTHOR CONTRIBUTIONS

T.G., H.W., and T.W. designed the research. T.G., H.W., M.C.E.N., L.T., O.N., and T.W. performed the research and analyzed the data. T.G. and T.W. wrote the paper.

ACKNOWLEDGMENTS

We thank Sören Werner and Thomas Schmülling for providing the *ATML1:CKX1-myc Arabidopsis* line, Bruno Müller for the *TCSn:GFP* reporter, Jianming Li for *ebs7-2*, and Jianru Zuo for the *35S:ARR15* line. The authors have no conflict of interest to declare.

Received: March 13, 2020

Revised: May 18, 2021

Accepted: July 21, 2021

Published: July 23, 2021

REFERENCES

- Antoniadi, I., Plačková, L., Simonovik, B., Doležal, K., Turnbull, C., Ljung, K., and Novák, O. (2015). Cell-type-specific cytokinin distribution within the *Arabidopsis* primary root apex. *Plant Cell* **27**:1955–1967.
- Bajguz, A., and Piotrowska, A. (2009). Conjugates of auxin and cytokinin. *Phytochemistry* **70**:957–969.
- Baldridge, R.D., and Rapoport, T.A. (2016). Autoubiquitination of the Hrd1 ligase triggers protein retrotranslocation in ERAD. *Cell* **166**:394–407.
- Barth, O., Vogt, S., Uhlemann, R., Zschiesche, W., and Humbeck, K. (2009). Stress induced and nuclear localized HIPP26 from *Arabidopsis thaliana* interacts via its heavy metal associated domain with the drought stress related zinc finger transcription factor ATHB29. *Plant Mol. Biol.* **69**:213–226.
- Bartrina, I., Jensen, H., Novák, O., Strnad, M., Werner, T., and Schmülling, T. (2017). Gain-of-function mutants of the cytokinin receptors AHK2 and AHK3 regulate plant organ size, flowering time and plant longevity. *Plant Physiol.* **173**:1783–1797.
- Bartrina, I., Otto, E., Strnad, M., Werner, T., and Schmülling, T. (2011). Cytokinin regulates the activity of reproductive meristems, flower organ size, ovule formation, and thus seed yield in *Arabidopsis thaliana*. *Plant Cell* **23**:69–80.
- Berner, N., Reutter, K.-R., and Wolf, D.H. (2018). Protein quality control of the endoplasmic reticulum and ubiquitin-proteasome-triggered degradation of aberrant proteins: yeast pioneers the path. *Annu. Rev. Biochem.* **87**:751–782.
- Bhargava, A., Clabaugh, I., To, J.P., Maxwell, B.B., Chiang, Y.-H., Schaller, G.E., Loraine, A., and Kieber, J.J. (2013). Identification of cytokinin-responsive genes using microarray meta-analysis and RNA-seq in *Arabidopsis*. *Plant Physiol.* **162**:272–294.
- Brenner, W.G., Ramireddy, E., Heyl, A., and Schmülling, T. (2012). Gene regulation by cytokinin in *Arabidopsis*. *Front. Plant Sci.* **3**:8.
- Caesar, K., Thamm, A.M.K., Witthöft, J., Elgass, K., Huppenberger, P., Grefen, C., Horak, J., and Harter, K. (2011). Evidence for the localization of the *Arabidopsis* cytokinin receptors AHK3 and AHK4 in the endoplasmic reticulum. *J. Exp. Bot.* **62**:5571–5580.
- Chuck, G., Lincoln, C., and Hake, S. (1996). *KNAT1* induces lobed leaves with ectopic meristems when overexpressed in *Arabidopsis*. *Plant Cell* **8**:1277–1289.
- Clough, S.J., and Bent, A.F. (1998). Floral dip: a simplified method for *Agrobacterium*-mediated transformation of *Arabidopsis thaliana*. *Plant J.* **16**:735–743.
- Cortleven, A., Leuendorf, J.E., Frank, M., Pezzetta, D., Bolt, S., and Schmülling, T. (2019). Cytokinin action in response to abiotic and biotic stresses in plants. *Plant Cell Environ.* **42**:998–1018.
- Cowan, G.H., Roberts, A.G., Jones, S., Kumar, P., Kalyandurg, P.B., Gil, J.F., Savenkov, E.I., Hemsley, P.A., and Torrance, L. (2018). Potato mop-top virus co-opts the stress sensor HIPP26 for long-distance movement. *Plant Physiol.* **176**:2052–2070.
- Crowell, D.N., and Huizinga, D.H. (2009). Protein isoprenylation: the fat of the matter. *Trends Plant Sci.* **14**:163–170.
- D'Agostino, I.B., Deruere, J., and Kieber, J.J. (2000). Characterization of the response of the *Arabidopsis* response regulator gene family to cytokinin. *Plant Physiol.* **124**:1706–1717.
- Dalal, J., Yalamanchili, R., La Hovary, C., Ji, M., Rodriguez-Welsh, M., Aslett, D., Ganapathy, S., Grunden, A., Sederoff, H., and Qu, R. (2015). A novel gateway-compatible binary vector series (PC-GW) for flexible cloning of multiple genes for genetic transformation of plants. *Plasmid* **81**:55–62.
- de Abreu-Neto, J.B., Turchetto-Zolet, A.C., de Oliveira, L.F.V., Bodanese Zanettini, M.H., and Margis-Pinheiro, M. (2013). Heavy metal-associated isoprenylated plant protein (HIPP): characterization of a family of proteins exclusive to plants. *FEBS J.* **280**:1604–1616.
- Dello Ioio, R., Linhares, F.S., Scacchi, E., Casamitjana-Martinez, E., Heidstra, R., Costantino, P., and Sabatini, S. (2007). Cytokinins determine *Arabidopsis* root-meristem size by controlling cell differentiation. *Curr. Biol.* **17**:678–682.

- Dortay, H., Gruhn, N., Pfeifer, A., Schwerdtner, M., Schmölling, T., and Heyl, A. (2008). Toward an interaction map of the two-component signaling pathway of *Arabidopsis thaliana*. *J. Proteome Res.* **7**:3649–3660.
- Dykema, P., Sipes, P., Marie, A., Biermann, B., Crowell, D., and Randall, S. (1999). A new class of proteins capable of binding transition metals. *Plant Mol. Biol.* **41**:139–150.
- Earley, K.W., Haag, J.R., Pontes, O., Opper, K., Juehne, T., Song, K., and Pikaard, C.S. (2006). Gateway-compatible vectors for plant functional genomics and proteomics. *Plant J.* **45**:616–629.
- Efroni, I., Han, S.-K., Kim, Hye J., Wu, M.-F., Steiner, E., Birnbaum, Kenneth D., Hong, Jong C., Eshed, Y., and Wagner, D. (2013). Regulation of leaf maturation by chromatin-mediated modulation of cytokinin responses. *Dev. Cell* **24**:438–445.
- Gao, W., Xiao, S., Li, H.-Y., Tsao, S.-W., and Chye, M.-L. (2009). *Arabidopsis thaliana* acyl-CoA-binding protein ACBP2 interacts with heavy-metal-binding farnesylated protein AtFP6. *New Phytol.* **181**:89–102.
- Geldner, N., Dénervaud-Tendon, V., Hyman, D.L., Mayer, U., Stierhof, Y.-D., and Chory, J. (2009). Rapid, combinatorial analysis of membrane compartments in intact plants with a multicolor marker set. *Plant J.* **59**:169–178.
- Gookin, T.E., and Assmann, S.M. (2014). Significant reduction of BiFC non-specific assembly facilitates *in planta* assessment of heterotrimeric G-protein interactors. *Plant J.* **80**:553–567.
- Hampton, R.Y., and Sommer, T. (2012). Finding the will and the way of ERAD substrate retrotranslocation. *Curr. Opin. Cell. Biol.* **24**:460–466.
- Hemsley, P.A. (2015). The importance of lipid modified proteins in plants. *New Phytol.* **205**:476–489.
- Holst, K., Schmölling, T., and Werner, T. (2011). Enhanced cytokinin degradation in leaf primordia of transgenic *Arabidopsis* plants reduces leaf size and shoot organ primordia formation. *J. Plant Physiol.* **168**:1328–1334.
- Howell, S.H. (2013). Endoplasmic reticulum stress responses in plants. *Annu. Rev. Plant Biol.* **64**:477–499.
- Hüttner, S., Veit, C., Vavra, U., Schoberer, J., Liebminger, E., Maresch, D., Grass, J., Altmann, F., Mach, L., and Strasser, R. (2014). *Arabidopsis* class I α -mannosidases MNS4 and MNS5 are involved in endoplasmic reticulum-associated degradation of misfolded glycoproteins. *Plant Cell* **26**:1712–1728.
- Hwang, I., and Sheen, J. (2001). Two-component circuitry in *Arabidopsis* cytokinin signal transduction. *Nature* **413**:383–389.
- Karimi, M., Inzé, D., and Depicker, A. (2002). GATEWAY vectors for *Agrobacterium*-mediated plant transformation. *Trends Plant Sci.* **7**:193–195.
- Kieber, J.J., and Schaller, G.E. (2018). Cytokinin signaling in plant development. *Development* **145**:dev149344.
- Köllmer, I., Novák, O., Strnad, M., Schmölling, T., and Werner, T. (2014). Overexpression of the cytosolic cytokinin oxidase/dehydrogenase (CKX7) from *Arabidopsis* causes specific changes in root growth and xylem differentiation. *Plant J.* **78**:359–371.
- Kosugi, S., Hasebe, M., Tomita, M., and Yanagawa, H. (2009). Systematic identification of cell cycle-dependent yeast nucleocytoplasmic shuttling proteins by prediction of composite motifs. *Proc. Natl. Acad. Sci. U S A* **106**:10171–10176.
- Laplaze, L., Benková, E., Casimiro, I., Maes, L., Vanneste, S., Swarup, R., Weijers, D., Calvo, V., Parizot, B., Herrera-Rodriguez, M.B., et al. (2007). Cytokinins act directly on lateral root founder cells to inhibit root initiation. *Plant Cell* **19**:3889–3900.
- Leibfried, A., To, J.P.C., Busch, W., Stehling, S., Kehle, A., Demar, M., Kieber, J.J., and Lohmann, J.U. (2005). WUSCHEL controls meristem function by direct regulation of cytokinin-inducible response regulators. *Nature* **438**:1172–1175.
- Lerich, A., Langhans, M., Sturm, S., and Robinson, D.G. (2011). Is the 6 kDa tobacco etch viral protein a bona fide ERES marker? *J. Exp. Bot.* **62**:5013–5023.
- Lin, L., Zhang, C., Chen, Y., Wang, Y., Wang, D., Liu, X., Wang, M., Mao, J., Zhang, J., Xing, W., et al. (2019). PAWH1 and PAWH2 are plant-specific components of an *Arabidopsis* endoplasmic reticulum-associated degradation complex. *Nat. Commun.* **10**:3492.
- Liu, Y., Zhang, C., Wang, D., Su, W., Liu, L., Wang, M., and Li, J. (2015). EBS7 is a plant-specific component of a highly conserved endoplasmic reticulum-associated degradation system in *Arabidopsis*. *Proc. Natl. Acad. Sci. U S A* **112**:12205–12210.
- Miyawaki, K., Matsumoto-Kitano, M., and Kakimoto, T. (2004). Expression of cytokinin biosynthetic isopentenyltransferase genes in *Arabidopsis*: tissue specificity and regulation by auxin, cytokinin, and nitrate. *Plant J.* **37**:128–138.
- Niemann, M.C.E., Bartrina, I., Ashikov, A., Weber, H., Novák, O., Spíchal, L., Strnad, M., Strasser, R., Bakker, H., Schmölling, T., et al. (2015). *Arabidopsis* ROCK1 transports UDP-GlcNAc/UDP-GalNAc and regulates ER protein quality control and cytokinin activity. *Proc. Natl. Acad. Sci. U S A* **112**:291–296.
- Niemann, M.C.E., Weber, H., Hluska, T., Leonte, G., Anderson, S.M., Novák, O., Senes, A., and Werner, T. (2018). The cytokinin oxidase/dehydrogenase CKX1 is a membrane-bound protein requiring homooligomerization in the endoplasmic reticulum for its cellular activity. *Plant Physiol.* **176**:2024–2039.
- Nishimura, C., Ohashi, Y., Sato, S., Kato, T., Tabata, S., and Ueguchi, C. (2004). Histidine kinase homologs that act as cytokinin receptors possess overlapping functions in the regulation of shoot and root growth in *Arabidopsis*. *Plant Cell* **16**:1365–1377.
- Oparka, K.J., Prior, D.A.M., Cruz, S.S., Padgett, H.S., and Beachy, R.N. (1997). Gating of epidermal plasmodesmata is restricted to the leading edge of expanding infection sites of tobacco mosaic virus (TMV). *Plant J.* **12**:781–789.
- Radakovic, Z.S., Anjam, M.S., Escobar, E., Chopra, D., Cabrera, J., Silva, A.C., Escobar, C., Sobczak, M., Grundler, F.M.W., and Siddique, S. (2018). *Arabidopsis* HIPP27 is a host susceptibility gene for the beet cyst nematode *Heterodera schachtii*. *Mol. Plant Pathol.* **19**:1917–1928.
- Ren, B., Liang, Y., Deng, Y., Chen, Q., Zhang, J., Yang, X., and Zuo, J. (2009). Genome-wide comparative analysis of type-A *Arabidopsis* response regulator genes by overexpression studies reveals their diverse roles and regulatory mechanisms in cytokinin signaling. *Cell Res* **19**:1178–1190.
- Resh, M.D. (2013). Covalent lipid modifications of proteins. *Curr. Biol.* **23**:R431–R435.
- Robinson, N.J., and Winge, D.R. (2010). Copper metallochaperones. *Annu. Rev. Biochem.* **79**:537–562.
- Romanov, G.A., Lomin, S.N., and Schmölling, T. (2018). Cytokinin signaling: from the ER or from the PM? That is the question!. *New Phytol.* **218**:41–53.
- Rost, B., Yachdav, G., and Liu, J. (2004). The PredictProtein server. *Nucl. Acids Res.* **32**:W321–W326.
- Rupp, H.M., Frank, M., Werner, T., Strnad, M., and Schmölling, T. (1999). Increased steady state mRNA levels of the *STM* and *KNAT1* homeobox genes in cytokinin overproducing *Arabidopsis thaliana* indicate a role for cytokinins in the shoot apical meristem. *Plant J.* **18**:557–563.
- Sakakibara, H. (2006). Cytokinins: activity, biosynthesis, and translocation. *Annu. Rev. Plant Biol.* **57**:431–449.

- Schmülling, T., Werner, T., Riefler, M., Krupková, E., and Bartrina y Manns, I. (2003). Structure and function of cytokinin oxidase/dehydrogenase genes of maize, rice, *Arabidopsis* and other species. *J. Plant Res.* **116**:241–252.
- Shani, E., Ben-Gera, H., Shleizer-Burko, S., Burko, Y., Weiss, D., and Ori, N. (2010). Cytokinin regulates compound leaf development in tomato. *Plant Cell* **22**:3206–3217.
- Sparkes, I.A., Runions, J., Kearns, A., and Hawes, C. (2006). Rapid, transient expression of fluorescent fusion proteins in tobacco plants and generation of stably transformed plants. *Nat. Protoc.* **1**:2019–2025.
- Strasser, R. (2018). Protein quality control in the endoplasmic reticulum of plants. *Annu. Rev. Plant Biol.* **69**:147–172.
- Suzuki, N., Yamaguchi, Y., Koizumi, N., and Sano, H. (2002). Functional characterization of a heavy metal binding protein Cdl19 from *Arabidopsis*. *Plant J.* **32**:165–173.
- Svačinová, J., Novák, O., Plačková, L., Lenobel, R., Holík, J., Strnad, M., and Doležal, K. (2012). A new approach for cytokinin isolation from *Arabidopsis* tissues using miniaturized purification: pipette tip solid-phase extraction. *Plant Methods* **8**:17.
- Tehseen, M., Cairns, N., Sherson, S., and Cobbett, C.S. (2010). Metallochaperone-like genes in *Arabidopsis thaliana*. *Metallomics* **2**:556–564.
- To, J.P.C., Haberer, G., Ferreira, F.J., Deruere, J., Mason, M.G., Schaller, G.E., Alonso, J.M., Ecker, J.R., and Kieber, J.J. (2004). Type-A *Arabidopsis* response regulators are partially redundant negative regulators of cytokinin signaling. *Plant Cell* **16**:658–671.
- Vandesompele, J., De Preter, K., Pattyn, F., Poppe, B., Van Roy, N., De Paepe, A., and Speleman, F. (2002). Accurate normalization of real-time quantitative RT-PCR data by geometric averaging of multiple internal control genes. *Genome Biol.* **3**, research0034.1. <https://doi.org/10.1186/gb-2002-3-7-research0034>.
- Voinnet, O., Rivas, S., Mestre, P., and Baulcombe, D. (2003). An enhanced transient expression system in plants based on suppression of gene silencing by the p19 protein of tomato bushy stunt virus. *Plant J.* **33**:949–956.
- Weber, H., Bernhardt, A., Dieterle, M., Hano, P., Mutlu, A., Estelle, M., Genschik, P., and Hellmann, H. (2005). *Arabidopsis* AtCUL3a and AtCUL3b form complexes with members of the BTB/POZ-MATH protein family. *Plant Physiol.* **137**:83–93.
- Weber, H., and Hellmann, H. (2009). *Arabidopsis thaliana* BTB/POZ-MATH proteins interact with members of the ERF/AP2 transcription factor family. *FEBS J.* **276**:6624–6635.
- Werner, S., Bartrina, I., Novák, O., Strnad, M., Werner, T., and Schmülling, T. (2021). The cytokinin status of the epidermis regulates aspects of vegetative and reproductive development in *Arabidopsis thaliana*. *Front. Plant Sci.* **12**:613488.
- Werner, T., Köllmer, I., Bartrina, I., Holst, K., and Schmülling, T. (2006). New insights into the biology of cytokinin degradation. *Plant Biol. (Stuttg.)* **8**:371–381.
- Werner, T., Motyka, V., Laucou, V., Smets, R., Van Onckelen, H., and Schmülling, T. (2003). Cytokinin-deficient transgenic *Arabidopsis* plants show multiple developmental alterations indicating opposite functions of cytokinins in the regulation of shoot and root meristem activity. *Plant Cell* **15**:2532–2550.
- Werner, T., and Schmülling, T. (2009). Cytokinin action in plant development. *Curr. Opin. Plant Biol.* **12**:527–538.
- Wu, X., and Rapoport, T.A. (2018). Mechanistic insights into ER-associated protein degradation. *Curr. Opin. Cell Biol.* **53**:22–28.
- Wulfetange, K., Lomin, S.N., Romanov, G.A., Stolz, A., Heyl, A., and Schmülling, T. (2011). The cytokinin receptors of *Arabidopsis* are located mainly to the endoplasmic reticulum. *Plant Physiol.* **156**:1808–1818.
- Yuan, C., Lazarowitz, S.G., and Citovsky, V. (2016). Identification of a functional plasmodesmal localization signal in a plant viral cell-to-cell-movement protein. *mBio* **7**:e02052-15.
- Zatloukal, M., Gemrotová, M., Doležal, K., Havlíček, L., Spíchal, L., and Strnad, M. (2008). Novel potent inhibitors of *A. thaliana* cytokinin oxidase/dehydrogenase. *Bioorg. Med. Chem.* **16**:9268–9275.
- Zschiesche, W., Barth, O., Daniel, K., Böhme, S., Rausche, J., and Humbeck, K. (2015). The zinc-binding nuclear protein HIPP3 acts as an upstream regulator of the salicylate-dependent plant immunity pathway and of flowering time in *Arabidopsis thaliana*. *New Phytol.* **207**:1084–1096.
- Zürcher, E., Liu, J., di Donato, M., Geisler, M., and Müller, B. (2016). Plant development regulated by cytokinin sinks. *Science* **353**:1027–1030.
- Zürcher, E., and Müller, B. (2016). Cytokinin synthesis, signaling, and function—advances and new insights. *Int. Rev. Cell Mol. Biol.* **324**:1–38.
- Zürcher, E., Tavor-Deslex, D., Lituiev, D., Enkeli, K., Tarr, P.T., and Müller, B. (2013). A robust and sensitive synthetic sensor to monitor the transcriptional output of the cytokinin signaling network in planta. *Plant Physiol.* **161**:1066–1075.